ONC201-Derived Tetrahydropyridopyrimidindiones as Powerful ClpP Protease Activators to Tackle Diffuse Midline Glioma

Morena Miciaccia,[|] Olga Maria Baldelli,[|] Cosimo G. Fortuna,[|] Gianfranco Cavallaro, Domenico Armenise, Anselma Liturri, Savina Ferorelli, Denise Muñoz, Alessandro Bonifazi, Francesca Rizzo, Antonella Cormio, Silvana Filieri, Giuseppe Micalizzi, Paola Dugo, Luigi Mondello, Anna Maria Sardanelli, Francesco Bruni, Paola Loguercio Polosa, Maria Grazia Perrone,* and Antonio Scilimati*

ACCESS | Metrics & More | Article Recommendations | Supporting Information

ABSTRACT: Pediatric diffuse intrinsic pontine glioma (DIPG), classified under diffuse midline glioma, is a deadly tumor, with no effective treatments. The human mitochondrial protease hClpP is a potential DIPG therapeutic target, and this study describes the synthesis of two new series of tetrahydropyridopyrimidindiones (THPPDs) as hClpP activators. Among the tested compounds, we have identified **36** (THX6) that shows a strong hClpP activation (EC_{50} = 1.18 μM) and good cytotoxicity in **ONC201**-resistant cells (IC_{50} = 0.13 μM). Studying the oxidation mechanisms on cell membranes, the treatment of DIPG cells with **36** (THX6) causes a change in levels of fatty acids (PUFAs, MUFAs, and SFAs) compared to untreated cells and dysregulates the level of proteins involved in oxidative phosphorylation, biogenesis, and mitophagy that lead to a global collapse of mitochondrial integrity and function suggesting this as the mechanism through which **36** (THX6) accomplishes its antitumor activity in DIPG cell lines.
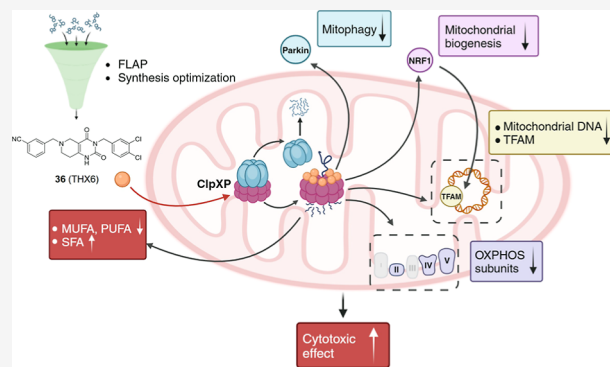
1. INTRODUCTION

Diffuse intrinsic pontine glioma (DIPG) according to the World Health Organization is a high-grade glioma (hGG) classified under diffuse midline gliomas (DMG).[1,2] This tumor typically arises in the pons of children aged 4−10 years and is very aggressive. Following diagnosis, usually confirmed by magnetic resonance imaging with a contrast medium, the mean progression-free survival is approximately 7 months, with an overall survival of about 3 months, regardless of the treatment administered. Symptoms of DIPG include impaired balance, strabismus, hemiparesis, eye movement disorders, facial muscle paralysis, and difficulty swallowing. Management of DIPG remains challenging due to the lack of a universally accepted and standardized treatment protocol. The current standard treatment involves radiotherapy, sometimes combined with various classes of drugs.[1] In a screen of approximately 2000 small molecules from the National Cancer Institute Chemical Library Diversity Set II, compound **ONC201** (formerly known as TIC10) (Figure 1) was identified as a p53-independent inducer of TRAIL-mediated apoptosis.[3,4] **ONC201** was proposed as a treatment for hGG, including DIPG, also because of its ability to cross the blood−brain barrier (BBB). Subsequent studies identified human caseinolytic protease hClpP as its target,

where **ONC201** acts as an allosteric activator.[5] A randomized, double-blind, placebo-controlled, parallel-group, international, phase III clinical trial is currently underway to evaluate the efficacy of **ONC201** in patients with newly diagnosed diffuse H3K27-altered glioma, following first-line radiotherapy.[6] Notably, **ONC201** induced regression of the primary thalamic lesion in a limited number of DMG patients.
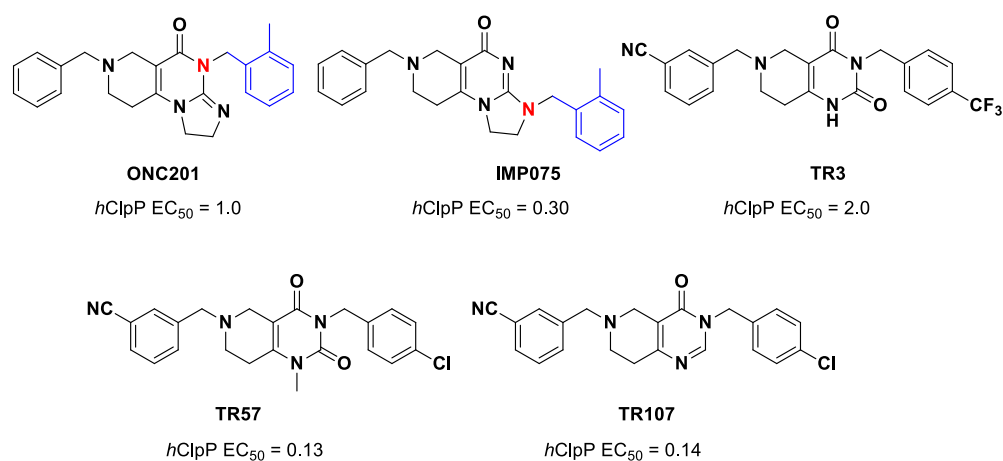
hClpP is a tetradecameric (two stacked heptameric rings) serine protease located in the mitochondrial matrix.[7,8] It plays a crucial role in mitochondrial proteostasis and is upregulated in numerous solid and hematological tumors, both primary and metastatic. In some cases, increased hClpP expression correlates with reduced patient survival.[9,10]

hClpP hydrolyzes misfolded and damaged proteins that are first recognized by the hexameric AAA+ unfoldase/translocase chaperone ClpX, forming the soluble complex ClpXP. As part of
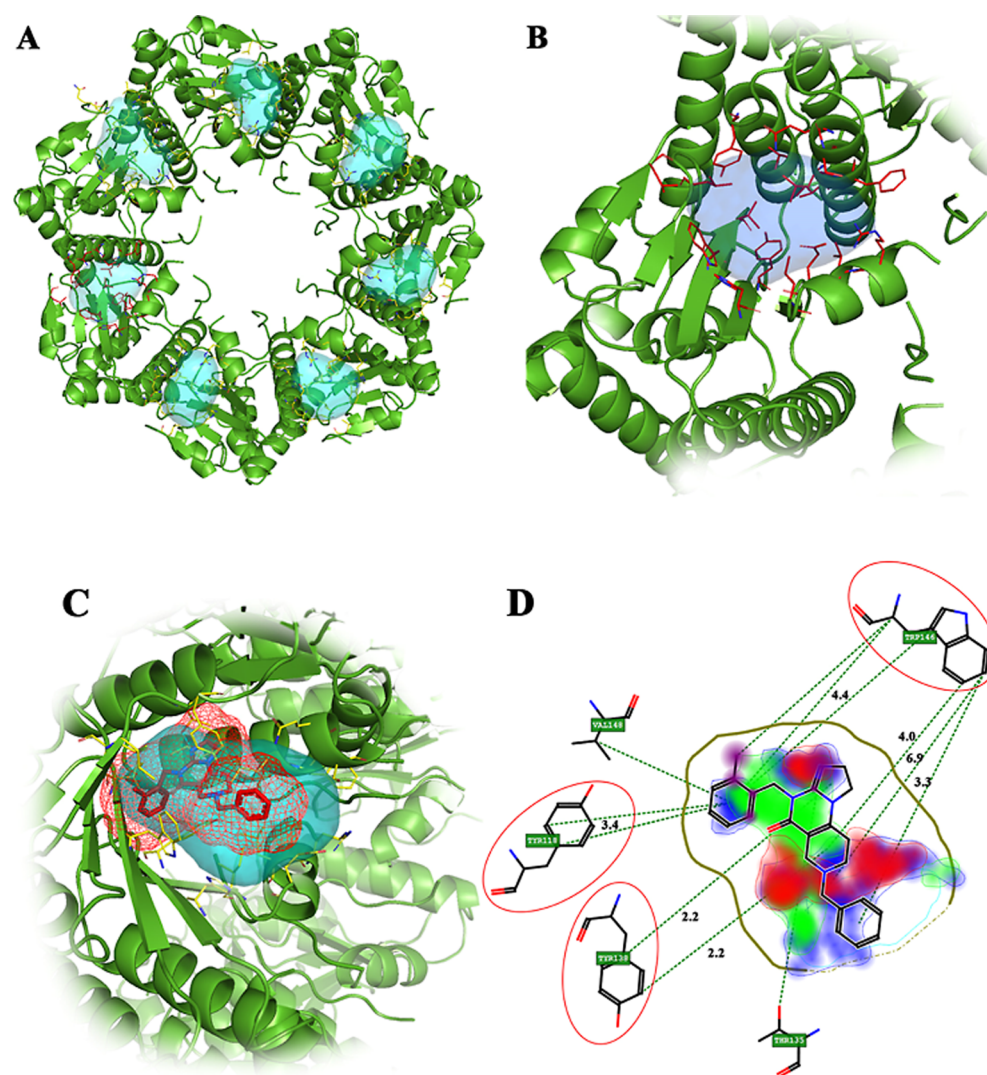
A

ONC201
hClpP EC$_{50}$ = 1.0

IMP075
hClpP EC$_{50}$ = 0.30

TR3
hClpP EC$_{50}$ = 2.0

TR57
hClpP EC$_{50}$ = 0.13

TR107
hClpP EC$_{50}$ = 0.14

Figure 1. Chemical structures of **ONC201**, **IMP075**, and some **TRs** representative [tetrahydropyridopyrimidindiones (THPPDs)].


Figure 2. hClpP:**ONC201** (PDB ID: 6DL7) complex crystal structure. (A) Top view of the seven pockets; (B) zoom view of one of the seven pockets randomly selected for virtual screening; (C) 3D binding pose and interaction area for **ONC201**; (D) 2D binding interactions with residues for **ONC201**.

the mitochondrial unfolded protein response system (UPRmt), ClpXP degrades misfolded or aggregated proteins in mammalian mitochondria maintaining organelle function and integrity and

affecting oxidative phosphorylation and mitochondrial metabolism in glioma cell lines and in other cancer models.[10,11]

ONC201 has a pharmacokinetic and pharmacodynamic profile, requiring further optimization. The dose used in clinical
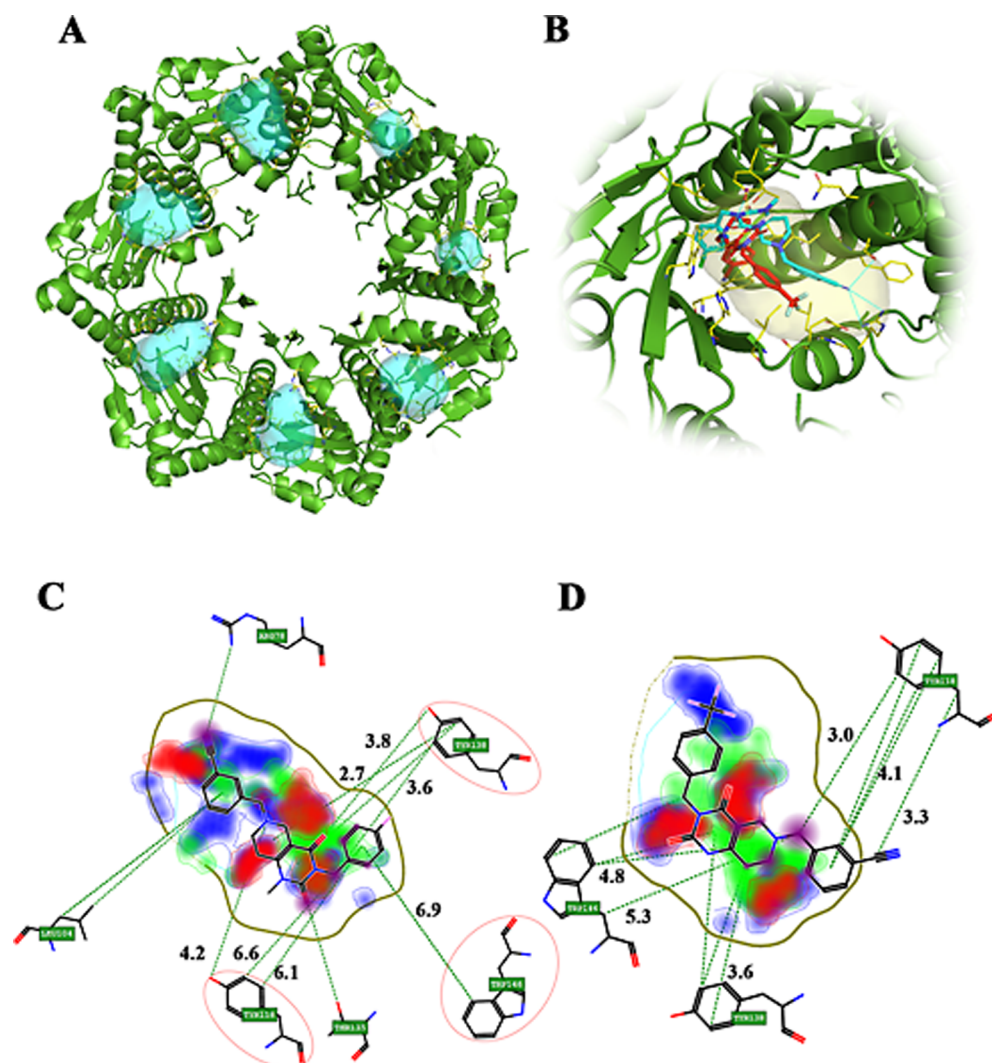
Figure 3. *h*ClpP:**TR57** (PDB ID: 7UVN) complex crystal structure. (A) Top view of seven pockets; (B) **TR57** (blue) and **TR3** (red) superimposed probes; (C) 2D binding interactions with residues of **TR57**; (D) 2D binding interactions with residues of **TR3**.

trials is relatively high, and not all the patients respond to treatment; moreover, **ONC201** antipsychotic effects must be considered because of its role as a dopamine D2 receptor antagonist (DRD2) presenting noncompetitive/negative allosteric pharmacology.[12]

Current investigations are aimed at better understanding the mechanism of action of **ONC201** and to identify novel compounds with improved pharmacological profiles. Consequently, a plenty of **ONC201** analogues have been synthesized, incorporating slight structural modifications to enhance efficacy.[1,13] Significant improvements in *h*ClpP activation were achieved by shifting the 2-methylbenzyl group from the amide to amine nitrogen atom (**IMP075**, Figure 1),[13,14] resulting in an order of magnitude increase in potency, whereas the attempt to simplify the **ONC201** chemical structure has led to the design a new class of *h*ClpP activators, known as **TR** derivatives (THPPDs), among which **TR57** was ∼10-fold more active than **ONC201** (Figure 1).[5,8,15]

In addition, **TR**s were found to be approximately 50−100 times more potent than **ONC201** in inhibiting the proliferation of HEK293 and MDA-MB-231 cell lines.[8]
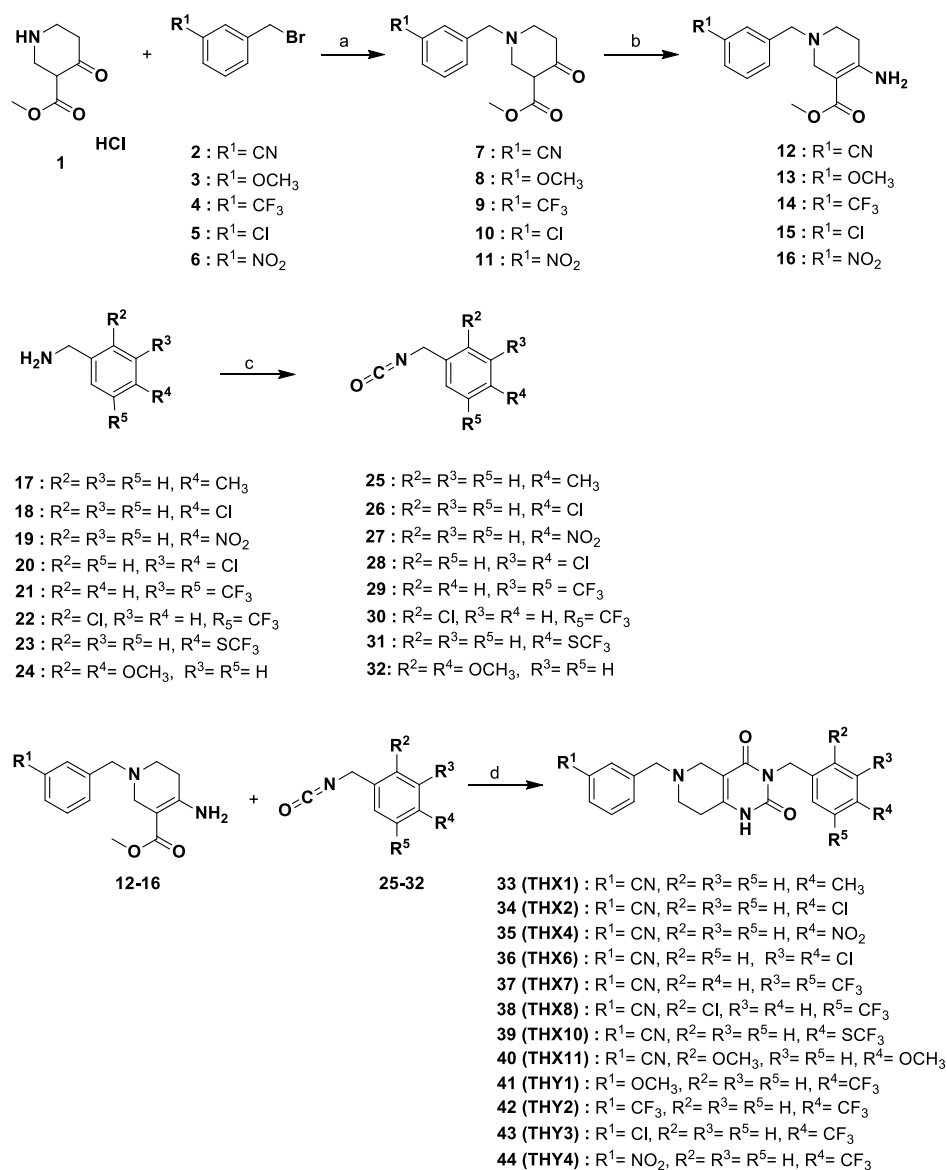
Herein, we describe the expansion of the number of compounds (two series called **THX** and **THY**) designed using

TR57/**TR3** as leads, also supported by *in silico* studies. Their toxicity on five DIPG cell lines (HSJD-DIPG-007, SU-DIPG-36, SU-DIPG-VI, SU-DIPG-50, and SF8628) with a different **ONC201** sensitivity and harboring a diverse mutated H3 isoform (H3.1K27- or H3.3K27-altered) was determined. All newly synthesized compounds have been evaluated for their capability to activate *h*ClpP; moreover, the effects on mitochondrial processes such as oxidative phosphorylation, biogenesis, and mitophagy in the SU-DIPG-36 cell line were also analyzed. Finally, the impact of the synthesized compounds on the lipid content of cell lines was also evaluated. In such a respect, gas chromatographic techniques coupled to mass spectrometry (GC−MS) and flame ionization detection (GC−FID) were used for the separation, identification, and quantification of the fatty acid methyl esters (FAMEs).

2. RESULTS AND DISCUSSION

2.1. Rational Design of the New Compounds. The *h*ClpP crystal structure in complex with **ONC201** (PDB ID: 6DL7; resolution, 2.00 Å)[16] was preliminarily used in fingerprints for ligands and proteins (FLAP) studies. The software identified 21 areas of interest (pockets), seven of which are symmetric (Figure 2A). The latter were taken into consideration

Scheme 1. Reagents and Conditions: (a) CH$_3$OH, K$_2$CO$_3$, r.t, 4 h; (b) NH$_3$·H$_2$O, EtOH, 70 °C, 5 h; (c) EtOAc, Triphosgene, 0−80 °C, 4 h; (d) Et$_3$N, Toluene, 80 °C, 16 h/MeONa, MeOH, Reflux, 16 h

17 : R^2= R^3= R^5= H, R^4= CH$_3$
18 : R^2= R^3= R^5= H, R^4= Cl
19 : R^2= R^3= R^5= H, R^4= NO$_2$
20 : R^2= R^5= H, R^3= R^4 = Cl
21 : R^2= R^4= H, R^3= R^5 = CF$_3$
22 : R^2= Cl, R^3= R^4 = H, R$_5$= CF$_3$
23 : R^2= R^3= R^5= H, R^4= SCF$_3$
24 : R^2= R^4= OCH$_3$, R^3= R^5= H

25 : R^2= R^3= R^5= H, R^4= CH$_3$
26 : R^2= R^3= R^5= H, R^4= Cl
27 : R^2= R^3= R^5= H, R^4= NO$_2$
28 : R^2= R^5= H, R^3= R^4 = Cl
29 : R^2= R^4= H, R^3= R^5 = CF$_3$
30 : R^2= Cl, R^3= R^4 = H, R$_5$= CF$_3$
31 : R^2= R^3= R^5= H, R^4= SCF$_3$
32: R^2= R^4= OCH$_3$, R^3= R^5= H

33 (THX1) : R^1= CN, R^2= R^3= R^5= H, R^4= CH$_3$
34 (THX2) : R^1= CN, R^2= R^3= R^5= H, R^4= Cl
35 (THX4) : R^1= CN, R^2= R^3= R^5= H, R^4= NO$_2$
36 (THX6) : R^1= CN, R^2= R^5= H, R^3= R^4= Cl
37 (THX7) : R^1= CN, R^2= R^4= H, R^3= R^5= CF$_3$
38 (THX8) : R^1= CN, R^2= Cl, R^3= R^4= H, R^5= CF$_3$
39 (THX10) : R^1= CN, R^2= R^3= R^5= H, R^4= SCF$_3$
40 (THX11) : R^1= CN, R^2= OCH$_3$, R^3= R^5= H, R^4= OCH$_3$
41 (THY1) : R^1= OCH$_3$, R^2= R^3= R^5= H, R^4=CF$_3$
42 (THY2) : R^1= CF$_3$, R^2= R^3= R^5= H, R^4= CF$_3$
43 (THY3) : R^1= Cl, R^2= R^3= R^5= H, R^4= CF$_3$
44 (THY4) : R^1= NO$_2$, R^2= R^3= R^5= H, R^4= CF$_3$

Scheme 2. Reagents and Conditions: (a) 5 bar H$_2$/Raney Nickel, 2N NH$_3$ in Ethanol, 20 °C, 16 h
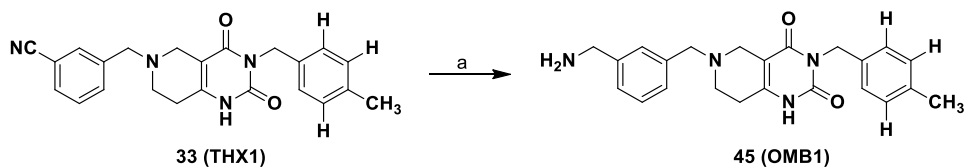

because they are those in which the ligand **ONC201** is cocrystallized. One of those seven was randomly selected to study the interactions established between *h*ClpP and the novel compounds (Figure 2B). Amino acids involved in the **ONC201**:*h*ClpP interaction include Arg78, Leu79, Glu82, Ile84, His116, Tyr118, Trp146, Val148, Leu170, Leu245, Ile100, Leu104, Phe105, Gln107, Ser108, Thr135, and Tyr138. The average of the distances of three key amino acid residues involved in the **ONC201**-pocket interaction was found to be 3.4 Å for Tyr118, 4.65 Å for Trp146, and 2.2 Å for Tyr138

highlighted in its 3D (Figure 2C) and 2D pose analysis (Figure 2D).

After determining with the software FLAP the exact binding mode of **ONC201** cocrystallized with *h*ClpP, it was tested whether the similar interaction model could be applied to **TR3** in order to use it as a "lead compound" to study the structural determinants that increase the proteolytic activity of *h*ClpP. Since the *h*ClpP:**TR3** complex is not yet reported, and due to the **TR3** and **TR57** high structural similarity, FLAP analysis was carried out by using X-ray data of the crystal *h*ClpP:**TR57** (PDB ID: 7UVN; resolution, 3.11 Å).[17] The results confirm that the

Table 1. FLAP Scores of ONC201, TR3, TR57, TR107, and 33−40 (THX)- and 41−45 (THY)-Sets of Compounds

compound	GLOB-SUM	GLOB-PROD	Distance	H	DRY	N1	O
ONC201	2.945	0.781	8.523	0.959	2.050	0.000	0.250
TR3	2.792	0.557	6.984	0.976	1.895	0.125	0.332
TR57	**3.141**	0.818	7.698	0.963	2.234	0.000	0.367
TR107	**3.103**	0.803	8.148	0.947	2.058	0.000	0.295
33 (THX1)	2.962	0.573	6.827	0.955	2.059	0.108	0.333
34 (THX2)	2.993	0.562	6.866	0.960	1.948	0.134	0.298
35 (THX4)	2.816	0.569	7.084	0.938	1.887	0.108	0.342
36 (THX6)	**3.192**	**0.599**	**6.268**	**0.967**	**2.131**	**0.121**	**0.364**
37 (THX7)	2.724	0.614	7.047	0.966	1.774	0.107	0.379
38 (THX8)	**3.124**	0.597	6.733	0.969	1.990	0.135	0.321
39 (THX10)	2.927	0.556	7.131	0.965	1.872	0.139	0.278
40 (THX11)	2.826	0.592	7.061	0.957	1.828	0.140	0.327
41 (THY1)	2.599	0.627	7.610	0.952	1.641	0.117	0.275
42 (THY2)	2.617	0.557	7.562	0.943	1.647	0.126	0.289
43 (THY3)	2.703	0.542	7.650	0.966	1.817	0.121	0.271
44 (THY4)	2.525	0.543	7.852	0.954	1.579	0.116	0.284
45 (OMB1)	**3.080**	0.681	5.806	0.962	1.913	0.205	0.333
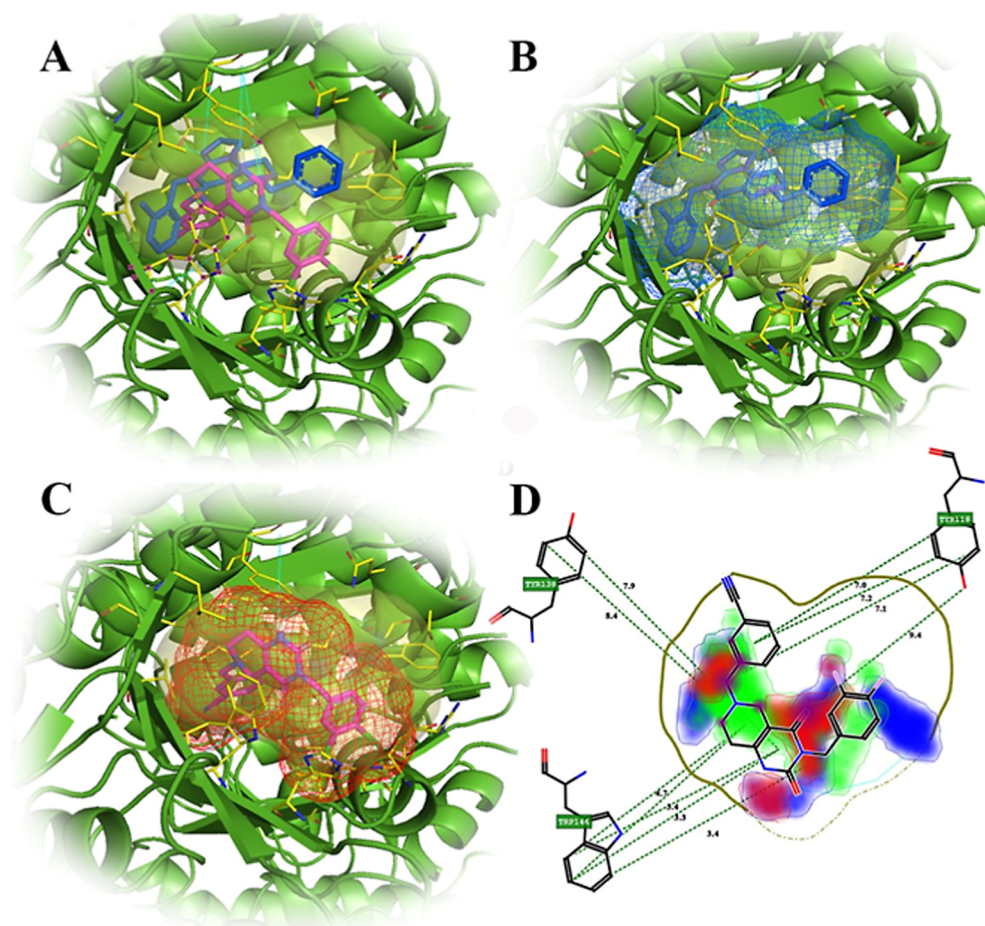
Figure 4. 3D binding poses of **ONC201** (blue) and **36** (THX6) (purple). (A) **ONC201** and **36** (THX6) 3D comparison poses. (B) 3D binding poses and interaction area for **ONC201**. (C) 3D binding poses and interaction area for **36** (THX6). (D) 2D binding poses for **36** (THX6). *h*ClpP:**ONC201** complex crystal structure (PDB ID: 6DL7).

THPPD ring of **TR3** is in the same position exactly where the pyrimidin-2,4-dione portion of **ONC201** is positioned (Figure 3).

This portion anchors the compound to the molecular surface of the enzyme *via* water-mediated hydrogen bonds, both in the backbone and in the side chain of Glu82 and Leu104. The

benzyls further stabilize the binding due to the presence of the cyano group spanning the backbone of Cys147 and the trifluoromethyl group opposite the guanidinium terminal of Arg78, respectively. Therefore, the pharmacophore organization of **TR3** is highly comparable to that of **ONC201**, prompting us to design some modifications of **TR3**. This led to the novel

Table 2. FLAP Scores of ONC201, TR57, TR3, TR107, and 36 (THX6) (PDB ID: 7UVN)

compound	GLOB-SUM	GLOB-PROD	Distance	H	DRY	N1	O
ONC201	2.823	0.752	8.901	0.971	1.815	0.000	0.282
TR57	**2.852**	0.839	8.283	0.973	1.746	0.000	0.333
TR3	2.702	0.568	7.646	0.966	1.650	0.120	0.290
TR107	2.804	0.782	8.810	0.958	1.747	0.000	0.293
36 (THX6)	**2.950**	0.579	6.770	0.962	2.010	0.131	0.319
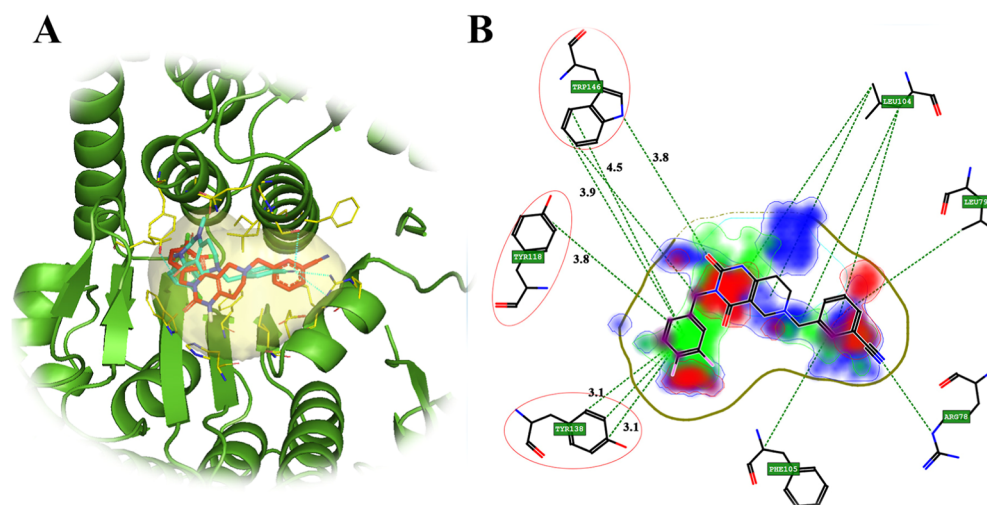
Figure 5. (A) **TR57** (light blue) and **36** (THX6) (red) 3D comparison poses (PDB ID: 7UVN); (B) 2D binding interactions with residues for THX6.

THPPDs series (33−45, Schemes 1 and 2) in which the group attached to the right-hand benzyl ring was modified, providing the THX series (33−40) and 45 (OMB1). Then, the group on the left-hand benzyl ring was changed, obtaining the THY series (41−44), leading to compounds that are differently potent in increasing the proteolytic activity of *h*ClpP (Table 3).

2.2. Chemistry. To prepare 7−11, the appropriate benzyl bromide (2−6) was added to a methanol solution of methyl-4-oxo-3 piperidine carboxylate hydrochloride (1) under basic conditions. Ketones (7−11) are transformed into the corresponding Schiff bases that, then, spontaneously convert into their enamine isomers 12−16. Following the reaction between the latter and the appropriate isocyanate (25−32), target compounds (33−44) were obtained. Isocyanates are prepared by reacting triphosgene and suitable benzylamine (17−24) (Scheme 1). 45 (OMB1) was prepared by reducing the cyano group with H_2/Raney-nickel in the presence of NH_3 (Scheme 2).
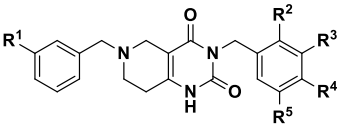
2.3. THX and THY Design Based on FLAP Analysis. FLAP identifies the molecular interaction fields (MIFs), using GRID calculations with four molecular probes: H (shape, steric effects), DRY (hydrophobic interactions), N1 (H-bond donor), and O (H-bond acceptor) interactions. In addition, the structure-based virtual screening (SBVS) mode provides three other important scores to evaluate the interactions: GLOB-SUM, GLOB-PROD, and Distance. The GLOB-SUM and GLOB-PROD scores refer to the summation and production of the interactions, respectively. The Distance score represents the overall similarity obtained by combining the degree of overlap between the individual probes (H, DRY, O, and N1) of the MIFs calculated for each candidate compound and the binding site; FLAP molecular probe scores based on the *h*ClpP:**ONC201** crystal structure are listed in Table 1.

The **ONC201**-GLOB-SUM score (2.945) was used as a reference to evaluate the degree of interaction of the target compounds 33−45 with *h*ClpP. Among all the new compounds, GLOB-SUM values higher than 3.0 were obtained for several compounds: 36 (THX6, 3.192), **TR57** (3.141), 38 (THX8, 3.124), **TR107** (3.103), and 45 (OMB1, 3.080). In Figure 4A, a comparison between the 3D poses of **ONC201** (blue) and 36 (THX6, purple) endowed with the highest GLOB-SUM value is shown. Focusing on their 3D and 2D poses (Figure 4B−D), 36 (THX6) demonstrates notable compatibility with the pocket compared to **ONC201**. 36 (THX6) bends and seemingly fits into the active site (Figure 3C), as supported by its H (0.967) and Distance (6.268) scores (**ONC201**'s H and Distance scores are 0.959 and 8.523, respectively). 36 (THX6) exhibits a sizable DRY (green area) and H-bond donor (blue area) interaction area (Figure 3D), which is larger than that of **ONC201**. Three amino acid residues (Tyr118, Trp146, and Tyr138), crucial for the **ONC201** interaction, are also essential for the 36 (THX6)−*h*ClpP interaction. The calculated average distances for these residues are 8.15, 3.7, and 7.68 Å for Tyr118, Trp146, and Tyr138, respectively (Figure 3D).

Similar interactions were detected carrying out FLAP by using the *h*ClpP:**TR57** crystal (PDB ID: 7UVN) (Table 2). GLOB-SUM scores for 36 (THX6) (2.95) and **TR57** (2.85) are also, in this case, the highest values of the considered compounds. Figure 5A,B shows a comparison of **TR57** and 36 (THX6) by 2D and 3D poses.

2.4. Evaluation of *h*ClpP Activity. Two sets of new compounds, 33−40 and 45 (OMB1) (THX series) and 41−44 (THY series), were prepared in discrete yields. THX compounds are characterized by the presence of an *m*-CN on the left benzyl, whereas THY compounds have different groups linked at both left and right benzyl positions. Their capability to increase the proteolytic activity of *h*ClpP was evaluated in a cell-

Table 3. 33−45 and References ONC201 and TR3 Biological Data, Percentage (%) Activation at 100 μM Normalized to the ONC201 Effect, and Calculated LogP by Consensus Log $P_{o/w}$ SwissADME[20]

compound	R^1	R^2	R^3	R^4	R^5	hClpP EC$_{50}$ (μM) $\pm$ SEM (% activation)[a]	ClogP
33 (THX1)	CN	H	H	CH$_3$	H	10.00 ± 0.10 (71)	3.74
34 (THX2)	CN	H	H	Cl	H	3.99 ± 0.10 (90)	3.94
35 (THX4)	CN	H	H	NO$_2$	H	7.70 ± 1.6 (87)	1.87
36 (THX6)	CN	H	Cl	Cl	H	1.18 ± 0.14 (97)	3.41
37 (THX7)	CN	H	CF$_3$	H	CF$_3$	16.0 ± 1.1 (44)	4.48
38 (THX8)	CN	Cl	H	H	CF$_3$	4.2 ± 0.4 (93)	3.89
39 (THX10)	CN	H	H	SCF$_3$	H	22.0 ± 2.1 (76)	3.75
40 (THX11)	CN	H	OCH$_3$	H	OCH$_3$	34.7 ± 1.6 (76)	2.35
41 (THY1)	OCH$_3$	H	H	CF$_3$	H	9.0 ± 3.1 (71)	3.68
42 (THY2)	CF$_3$	H	H	CF$_3$	H	3.80 ± 0.6 (96)	4.60
43 (THY3)	Cl	H	H	CF$_3$	H	4.7 ± 1.1 (100)	4.15
44 (THY4)	NO$_2$	H	H	CF$_3$	H	2.88 ± 0.24 (84)	3.04
45 (OMB1)	CH$_2$NH$_2$	H	H	CH$_3$	H	>100	2.32
TR3	CN	H	H	CF$_3$	H	2.0 ± 0.9 (100)	3.48
ONC201[b]						5.90 ± 2.5 (100)	2.99

[a]EC$_{50}$ values are presented as means $\pm$ SEM from at least 3 independent experiments, each performed in triplicate. [b]ONC201 chemical structure is depicted in Figure 1.
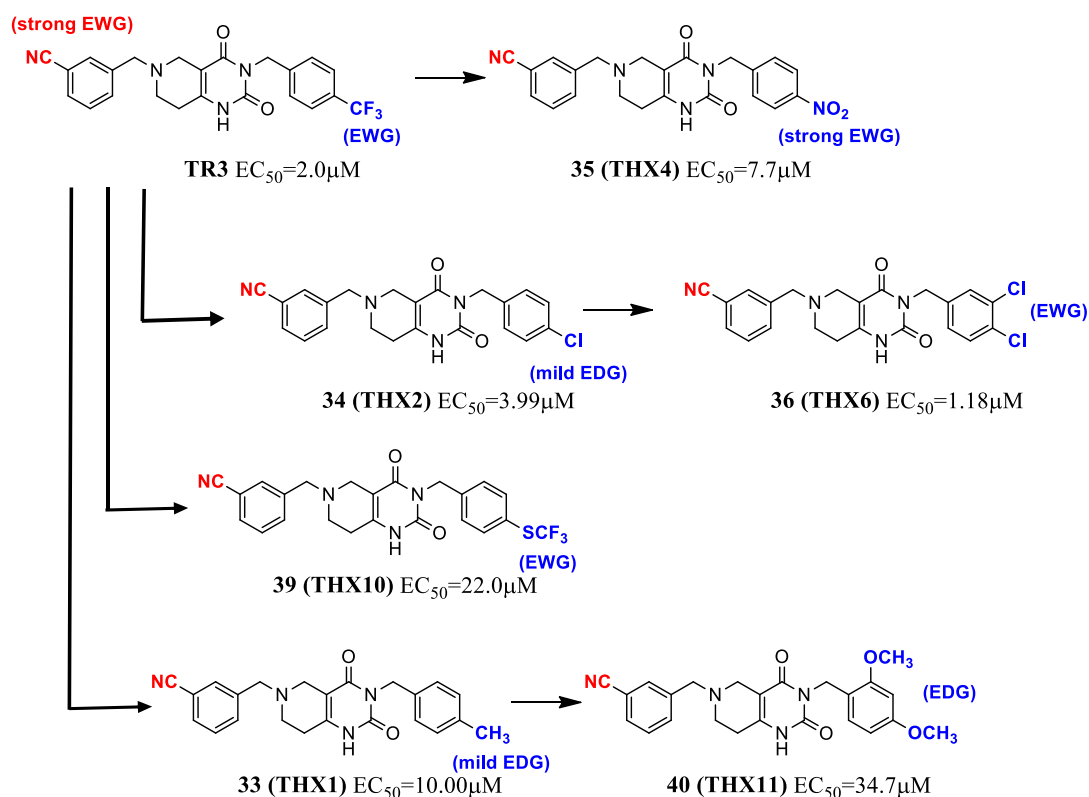
Figure 6. THX (33−40) series EC$_{50}$ values tree.

free assay using the fluorogenic protein substrate fluorescein-isothiocyanate (FITC)-casein (Table 3).[18,19] ONC201 and TR3 were used as references, showing EC$_{50}$ = 5.9 and 2.0 μM, respectively. ONC201 was chosen because it is the first compound to receive FDA fast-track designation for clinical use for the treatment of hGG, while TR3 is a prototype of the THX and THY series. Among the THX series designed with the

consideration of FLAP prediction (Tables 1 and 2), compound 36 (THX6, R^3 = R^4 = Cl) with an EC$_{50}$ of 1.18 μM is 5- and 1.7-fold more potent than ONC201 and TR3, respectively. Compounds 33 (THX1, R^4 = CH$_3$) and 34 (THX2, R^4 = Cl) have quite different EC$_{50}$ values of 10.0 and 3.99 μM, despite similar ClogP (3.74 and 3.94) but an opposite electronic effect on the aromatic ring; in particular, R^4 = CH$_3$ in 33 (THX1) is a

(strong EWG) NC

TR3 $EC_{50}=2.0\mu M$

(strong EWG) O_2N

44 (THY4) $EC_{50}=2.88\mu M$

(EWG) F_3C

42 (THY2) $EC_{50}=3.80\mu M$

(mild EDG) Cl

43 (THY3) $EC_{50}=4.7\mu M$

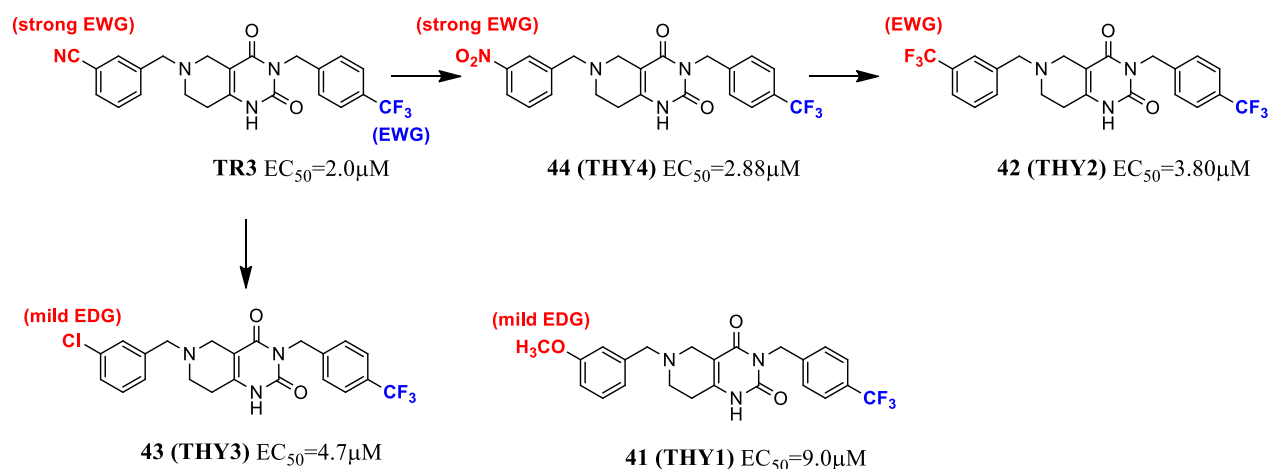(mild EDG) H_3CO

41 (THY1) $EC_{50}=9.0\mu M$

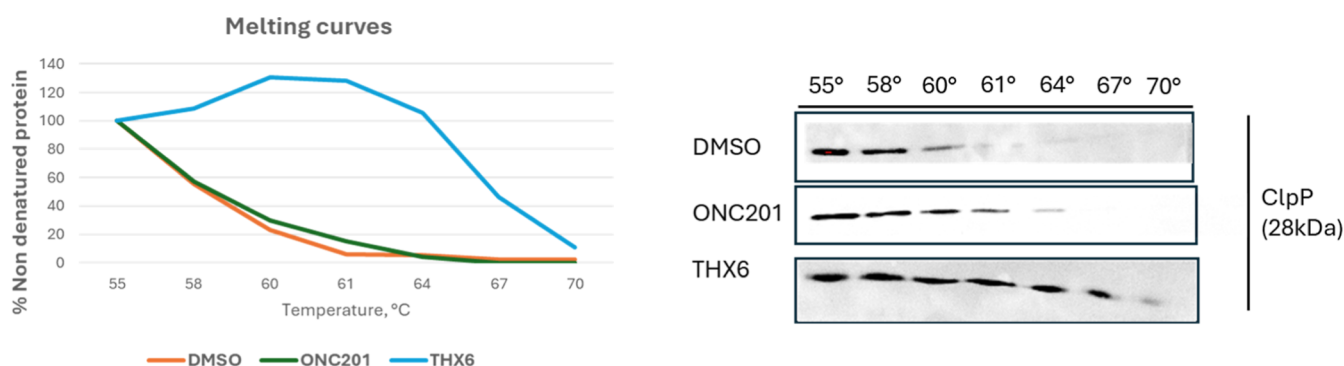**Figure 7.** THY (41−44) series EC_{50} values tree.

Figure 8. hClpP protein stability in the presence of **ONC201** or **36** (THX6) (CETSA). Melting curves (left panel) are based on hClpP protein expression (right panel) relative to the intensity at 55 °C.

mild electro-donating (ED) group due to hyperconjugation and the higher electronegativity of the carbon atom of the aromatic-ring-hybridized sp^2 than the carbon atom of the methyl-hybridized sp^3, instead R^4 = Cl in **34** (THX2) exerts a mild electro-withdrawing (EW) effect. The presence of an additional EWG in the meta-position causes a drastic reduction in potency, as seen with compounds **37** (THX7, R^3 = R^5 = CF_3) and **38** (THX8, R^2 = Cl, R^5 = CF_3), which have EC_{50} values of 16.0 and 4.2 μM, respectively. Compound **39** (THX10, R^4 = SCF_3) bearing a mild EW group has an EC_{50} = 22 μM. These compounds have similar ClogP values of 3.89 and 3.75. Compound **40** (THX11, R^3 = R^5 = OCH_3), another mild EDG, has an EC_{50} = 34.7 μM. In the THY series, compound **41** (THY1, R^1 = OCH_3, R^4 = CF_3) has an EC_{50} = 9.0 μM and a ClogP = 3.68. Compounds **42** (THY2, R^1 = R^4 = CF_3), bearing two trifluoromethyls, and **43** (THY3, R^1 = Cl, R^4 = CF_3), with one chlorine atom and one trifluoromethyl group in the same positions, have similar EC_{50} values of 3.8 and 4.7 μM, respectively. The presence of R^2 = NO_2 and R^4 = CF_3 in compound **44** (THY4) results in an EC_{50} of 2.88 μM, comparable to the EC_{50} value of **TR3**. Compound **45** (OMB1, R^2 = CH_2NH_2 and R^4 = CF_3) has no effect on the hClpP proteolytic activity (EC_{50} > 100 μM) and a very low ClogP value of 2.32.

In summary, within the THX series (**33−40**), the replacement of CF_3 in **TR3** by either EWG or EDG did not increase the hClpP proteolytic activity except for compound **36** (THX6) (Figure 6 and Table 3), confirming the FLAP prediction (Table 1 and Table 2).

The THY series (**41−44**) confirmed the importance of a strong EWD. Specifically, replacing the cyano group with a nitro group (conversion of **TR3** into **44** (THY4)) maintained the activation potency nearly unchanged (Figure 7 and Table 3). The other substitutions did not result in significant variations in the EC_{50} values.

2.5. hClpP Thermal Stability. Hydrolytic enzymes are stable and retain their catalytic activity under extreme conditions, such as temperatures exceeding 50 °C and in nonaqueous solvents.[21,22]

Cellular Thermal Shift Assay (CETSA) is a valuable method for investigating hClpP engagement within its complex cellular environments, since many proteins denature and aggregate when subjected to increasing temperatures. As protein aggregates are insoluble, this causes a shift from soluble to insoluble fractions. By quantifying the amount of remaining soluble protein at each temperature, the melting curve of hClpP can be generated and the point where the protein remains soluble can be identified. Stabilization of hClpP by the presence of binding activators such as **ONC201** and **36** (THX6) determines a shift in the thermal stability of the enzyme. The process for performing a CETSA on human colon carcinoma cells (Caco-2) is illustrated in Figure 8. hClpP was stabilized in the presence of **36** (THX6) and, to a lesser extent, by **ONC201**. This stabilization was evident from the hClpP melting curves and Western blot assay. CETSA band intensities were normalized to 100% with hClpP remaining in the supernatant at 55 °C set to 100% and subsequent bands expressed as a percentage thereof.

H

2.6. Evaluation of D2R and D3R Affinity. Knowing that **ONC201** was reported as a D2R/D3R antagonist, displaying noncompetitive/negative allosteric activity, the affinity of selected novel compounds was determined. The D2R/D3R affinity (K_i) of **33** (THX1), **36** (THX6), and **4** (THY4), alongside **TR3** and **ONC201**, used as references, was measured. The novel compounds showed no affinity for D2R, up to 100 μM, and an affinity for D3R equal to 31.4 μM for **33** (THX1), 51.1 μM for **36** (THX6), 26.7 μM for **44** (THY4), and 36.4 μM for **TR3**. **ONC201** presented moderate affinity for D2R and D3R (Table 4).[12,23]

Table 4. hD2R and hD3R Competition Binding in HEK293 Cells for Selected Novel hClpP Activators (33, 36, and 44) and References ONC201 and TR3

compound	hD2R	hD3R
	K_i (μM) $\pm$ SEM[a]	
33 (THX1)	>100	31.4 $\pm$ 1.49
36 (THX6)	>100	51.1 $\pm$ 1.52
44 (THY4)	>100	26.7 $\pm$ 5.86
ONC201	14.8 $\pm$ 1.40	4.09 $\pm$ 0.690
TR3	>100	36.4 $\pm$ 7.51

[a]K_i values were determined by competitive inhibition of [³H]N-methylspiperone binding in membranes harvested from HEK293 cells stably expressing hD2R and hD3R. K_i values are presented as means $\pm$ SEM from at least 3 independent experiments, each performed in triplicate.[24]

2.7. DIPG Cell Lines Cytotoxicity with Different ONC201 Sensitivity. The cytotoxicity of **ONC201** and **TR3** and all newly synthesized compounds (**33**−**45**) was evaluated on two DIPG cell lines with a different sensitivity to **ONC201**[25] and with H3.1K27M/H3.3K27M mutation representing the disease with different characteristics (Table 5). H3K27M mutation causes epigenetic silencing, although its precise role in tumorigenesis remains to be clarified. Mutated isoforms H3.1 and H3.3 influence differently survival, phenotype, and clinical outcomes. Specifically, histone H3.1 mutations are generally

Table 5. Cytotoxic Effect of ONC201, TR3, and 33−45 on SU-DIPG Cell Lines Determined Using CCK-8 Assay[a]

compound	SU-DIPG-36 H3.1K27M	SU-DIPG-50 H3.3K27M
	$IC_{50} \pm$ SEM, μM (% proliferation inhibition)	
ONC201	37 $\pm$ 2.5 (82)	25 $\pm$ 12.3 (66)
TR3	25.9 $\pm$ 0.03 (72)	22.8 $\pm$ 2.66 (68)
33 (THX1)	30 $\pm$ 1.0 (72)	29 $\pm$ 1.0 (41)
34 (THX2)	73 $\pm$ 2.5 (83)	>100 (36)
35 (THX4)	>100 (59)	>100 (35)
36 (THX6)	47.7 $\pm$ 7.2 (81)	>100 (39)
37 (THX7)	>100 (65)	>100 (77)
38 (THX8)	>100 (58)	>100 (61)
39 (THX10)	>100 (81)	>100 (77)
40 (THX11)	37 $\pm$ 2.5 (65)	36 $\pm$ 1.8 (40%)
41 (THY1)	80.2 $\pm$ 6.7 (85)	59.2 $\pm$ 8.5 (65%)
42 (THY2)	27.6 $\pm$ 5.2 (85)	20.0 $\pm$ 6.3 (66%)
43 (THY3)	60.7 $\pm$ 9.8 (86)	52.7 $\pm$ 12.3 (56%)
44 (THY4)	46.2 $\pm$ 18 (84)	17.4 $\pm$ 1.87 (69%)
45 (OMB1)	>100 (73)	>100 (67)

[a]Data are expressed as the mean of three independent experiments, and SEM values are reported.

associated with a slightly longer survival and reduced metastasis. Prognosis is poor in the presence of the mutations, regardless of the isoform involved (Table 5).[1,2,25−27] Even in our experimental conditions, **ONC201** was revealed to be more effective in the SU-DIPG-36 cell line with an IC_{50} of 37 μM reaching 82% of cell death compared to SU-DIPG-50, in which cell death is only of 66% with an IC_{50} of 25 μM. As for **ONC201**, all the other analyzed compounds had an efficacy higher in the SU-DIPG-36 cell line, particularly an IC_{50} lower than 100 μM was registered for all the THY series (**41**−**44**) and for **33**, **34**, **36**, and **40** of THX series (Table 5).

The cytotoxic potency of all synthesized compounds was on the order of micromolar magnitude, indicating that the antiproliferative effects are comparable. **36** (THX6) was the most potent hClpP activator and it was chosen to be tested in other DIPG cell lines and compared to **ONC201** and **TR3** (Table 6).

Table 6. TR3 and 36 (THX6) Cytotoxic Effect in DIPG Cell Lines That Show Variable Response to ONC201 Treatment

	Low		High
	ONC201-RESISTANCE		
Cell line	**HSJD-007**	**SF8628**	**SU-DIPG-VI**
mutation	H3.3K27M	H3.3K27M	H3.3K27M
source	autopsy	biopsy	autopsy
	$IC_{50}\mu$M		
ONC201	1.27$\pm$0.07	5.82$\pm$0.31	32.3$\pm$4.70
TR3	0.41$\pm$0.13	6.37$\pm$0.89	34.27$\pm$7.96
36 (THX6)	0.46$\pm$0.06	468$\pm$1.15	10.89$\pm$0.02

Jackson et al.[25] reported that the SU-DIPG-VI cell line does not respond to the treatment with **ONC201**, while HSJD-007 are sensitive to the action of imipridone, reporting an IC_{50} value of 2.13 μM; no data are available regarding the commercial DIPG cell line SF8628. In our experimental conditions, SU-DIPG-VI was confirmed to be the most **ONC201**-resistant cell line (IC_{50} = 32.3 μM), followed by SF8628 (IC_{50} = 5.82 μM) and HSJD-007 (IC_{50} = 1.27 μM). The same behavior was observed for **TR3** and **36** (THX6); a slightly higher efficacy of **36** in SU-DIPG-VI is noteworthy (Table 6).

2.8. Membrane Permeability of ONC201, 33, 35, 36, and 41−44. The membrane crossing rate, which considers both passive and active transport, is explicated through the apparent permeability coefficient (Papp). Papp is measured by using a monolayer of Caco-2,[28−31] which endogenously expresses a variety of carrier proteins present in various endothelial and epithelial barriers of the body. In particular, the P-gp efflux pumps present at the BBB are responsible for a limitation in drug membrane crossing. The Caco-2 cell monolayer is polarized to express P-gp only apically; thus, the basolateral-apical direction value (PappBA) refers to the rate at which compounds cross the membrane only considering their chemical−physical properties (passive transport). The compound that crosses the monolayer fastest is **TR3** which has a PappBA of 3385 nm/s followed by **33** (THX1) (2894 nm/s) and **ONC201** (2157 nm/s). On the contrary, the apical-

basolateral direction value (PappAB) represents the crossing rate in the presence of efflux pumps, specifically P-gp. In fact, the flux rate is always reduced compared to that of PappBA, since the compounds are partially retained by the efflux pumps. **33** (THX1) (905 nm/s) and **TR3** (759 nm/s) are least retained. **41** (THY1), **ONC201**, **44** (THY4), **42** (THY2), and **36** (THX6) are moderately retained, showing a flux rate of 287−356 nm/s **43** (THY3) and **35** (THX4) were the most retained, having a crossing rate lower than 250 nm/s (Table 7).

Table 7. Apparent Permeability (P_{app})^{a} Values of 33, 35, 36, 41−44, ONC201, and TR3

compound	P_{app}BA (nm/s)	P_{app}AB (nm/s)
33 (THX1)	2894 ± 111	905 ± 27
35 (THX4)	1024 ± 35	150 ± 2
36 (THX6)	459 ± 18	287 ± 8
41 (THY1)	1210 ± 35	403 ± 18
42 (THY2)	499 ± 11	302 ± 9
43 (THY3)	915 ± 21	223 ± 11
44 (THY4)	1184 ± 38	346 ± 9
ONC201	2157 ± 98	356 ± 12
TR3	3385 ± 110	759 ± 5

^{a}Data are expressed as the mean of three independent experiments, and SEM values are reported.

2.9. 36 (THX6) Effect on Mitochondrial Oxidative Phosphorylation, Biogenesis, and Mitophagy in the SU-DIPG-36 Cell Line. *2.9.1. Integrity of the ClpXP Complex.* As proven above, **36** (THX6) was found to be a highly potent activator of purified recombinant *h*ClpP expressed in bacteria.[19] Therefore, it seemed appropriate to evaluate its effect on mitochondrial processes such as oxidative phosphorylation, biogenesis, and mitophagy in the SU-DIPG-36 cell line, which was treated with **36** (THX6) for 24 h at a concentration close to its *h*ClpP EC$_{50}$ value (Table 3).

*h*ClpXP activators, such as **ONC201** and ADEPs, are known to displace the ATP-dependent ClpX chaperone from the *h*ClpXP complex and bind each *h*ClpP subunit, resulting in the widening of the central substrate cavity.[7] This promotes the proteolytic activity independent of the ClpX chaperone, followed by the rapid degradation of ClpX.

The levels of *h*ClpX and *h*ClpP were measured in the SU-DIPG-36 cell line treated with **36** (THX6) to analyze its effect on the integrity of the *h*ClpXP complex. First, it was assessed whether the compound could cause the *h*ClpX downregulation, an event generally considered a typical marker of aberrantly active *h*ClpP.[32] The level of the chaperone subunit was strongly decreased in response to **36** (THX6) (Figure 9A,B), suggesting that similar to other protease activators, it probably promotes the displacement of *h*ClpX from the peptidase component *h*ClpP, inducing selective degradation of the chaperone subunit. It is known that uncontrolled *h*ClpP activity could be responsible for the degradation of its own regulatory subunit, although the intervention of additional proteases of the mitochondrial matrix cannot be excluded.[33] Still, it remains unknown whether *h*ClpX downregulation is critical for the functioning of *h*ClpP activators or instead represents an unrelated secondary effect.

The decrease in the level of *h*ClpX induced by **36** (THX6) treatment did not appear to affect the amount of *h*ClpP, which remained essentially unchanged after 24 h of exposure to the compound (Figure 9A,B). Our data are in agreement with the

observations reported by others in different tumor cell lines and for longer exposure.[33]

2.9.2. OXPHOS Function, Mitochondrial Biogenesis, and Mitophagy. Several proteins, involved in mitochondrial OXPHOS, have been identified as substrates of *h*ClpP.[34] Therefore, we analyzed the effect of **36** (THX6) on the level of some respiratory chain subunits such as SDHA and ATP5A, which are nuclear-encoded subunits of complexes II and V, respectively, and COI, which is a mitochondrial (mt) DNA-encoded subunit of complex IV. A strong decline of all subunits' level, in particular, COI, was observed (Figure 9A,B). Such downregulation, which had already been documented for a wide variety of cancer cell models treated with **ONC201**, could cause the collapse of mitochondrial bioenergetics.[14,35]

The effect of *h*ClpP activation on some regulatory factors that control mitochondrial biogenesis, such as NRF1 and TFAM, was investigated. The signaling cascade of mitochondrial biogenesis is initiated by activation in the nucleus of PGC-1 alpha, resulting in NRF1 stimulation. This in turn stimulates transcription and expression of the mitochondrial protein TFAM, which plays an essential role in maintaining mtDNA genome integrity, copy number, transcription, and mtDNA replication.[36] Immunoblot experiments (Figure 9A, B) indicate that treatment of cells with compound **36** (THX6) for 24 h significantly diminished the level of NRF1 and, more markedly, TFAM.

Since NRF1 and TFAM are both differently important for the maintenance of mtDNA, their depletion following **36** (THX6) treatments prompted us to measure mtDNA relative levels in SU-DIPG-36 cells. Effectively, the mtDNA copy number was decreased, in agreement with the diminished levels of the two factors (Figure 9C). Overall, these data indicate that mitochondrial biogenesis and mtDNA maintenance were dysregulated when SU-DIPG-36 cells were treated with compound **36** (THX6).

On the other hand, the downregulation of TFAM, as early as 24 h, could result from proteolysis by hyperactivated *h*ClpP, considering that TFAM was identified as a direct substrate of **TR65**-activated ClpP.[8] Moreover, TFAM was shown to be a potential ClpP interactor by BioID interaction analyses.[37] Direct TFAM degradation by chemically activated ClpP was reported in breast and endometrial cancer cell lines exposed to the imipridone **ONC201**, showing a reduction of the TFAM level already within 6 h, which preceded that of its transcript.[35] Therefore, the TFAM decrease is likely contributed by a combination of proteolysis and perturbation of mitochondrial biogenesis.

To further confirm the effect of **36** (THX6) on mitochondrial biogenesis, we measured the level of TOMM20, which is a subunit of the mitochondrial outer membrane translocator, commonly used as a marker of mitochondrial content (Figure 9B); actually, a mitochondrial mass decrease was observed.

Finally, given the regulatory roles of *h*ClpXP in mitophagy,[38,39] we sought to assess the effect of *h*ClpP hyperactivation on mitochondria degradation. Mitophagy is driven by specialized proteins that, by sensing distinct extra-/intracellular signals, help in the recognition of superfluous or dysfunctional mitochondria by the autophagic machinery. We measured the levels of mitophagy markers such as Parkin, BNIP3, and NIX. A marked reduction of the Parkin level was detected in lysates of SU-DIPG cells treated with **36** (THX6) (Figure 9D,E). Such a decrease could be the result of a series of events that begin within mitochondria with the massive proteolytic cleavage of PINK1 by
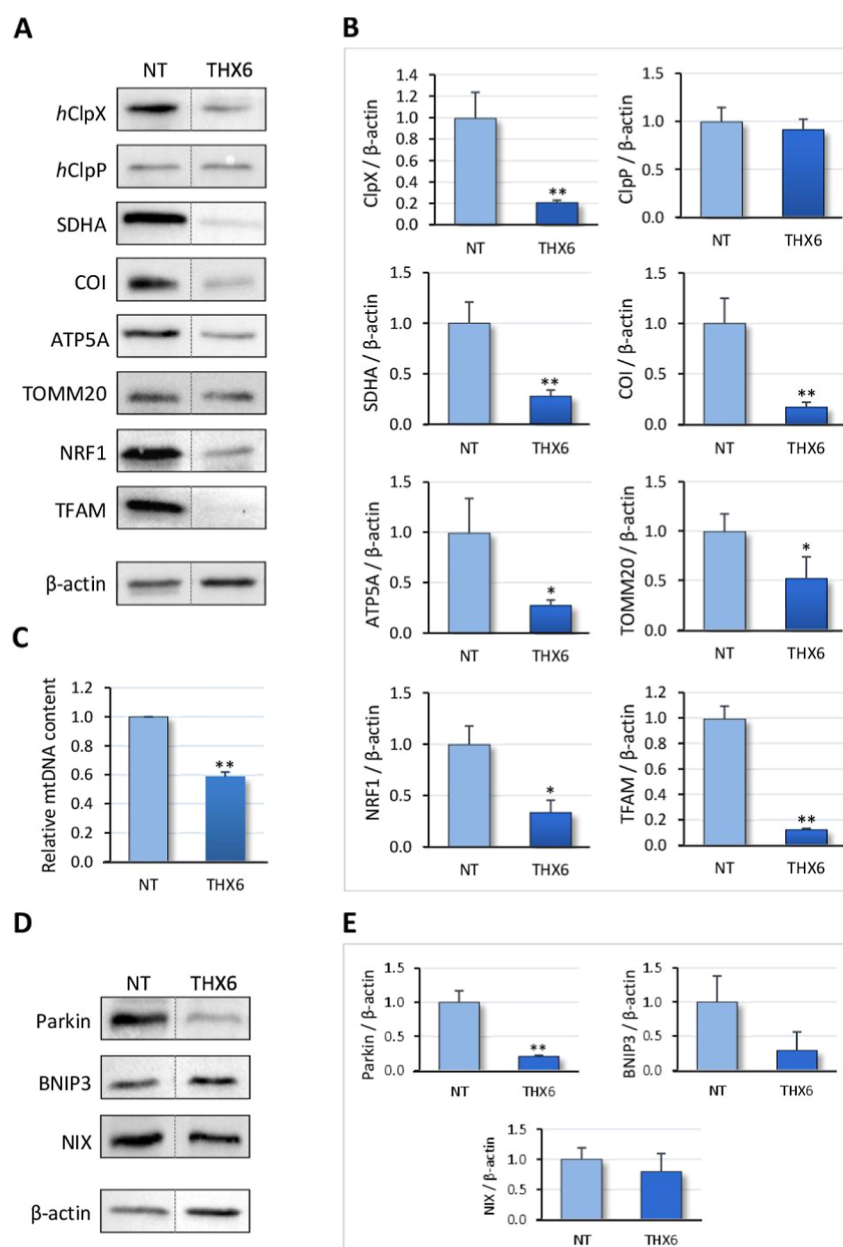
Figure 9. Molecular analysis of **36** (THX6) effects in SU-DIPG-36 cells. (A) Immunoblotting of whole cell lysates from untreated and **36** (THX6)-treated cells. (B) Relative quantification of proteins shown in panel A, normalized to β-actin. Results are presented as the mean ± SEM ($n = 4$). (C) Relative mtDNA content of the treated SU-DIPG-36 compared to untreated cells. Results are presented as the mean ± SD ($n = 3$). (D) Western blot analysis of mitophagy protein markers. (E) Relative quantification of proteins shown in panel (D), normalized to β-actin. Statistical analyses in (B,C,E) were performed using the Student's t tests (*, $p < 0.05$; **, $p < 0.01$).

hyperactivated hClpP. Cleaved PINK1 is released into the cytoplasm, where it binds cytosolic Parkin and promotes its degradation, downregulating mitophagy.[40] Immunoblotting of BNIP3 and NIX yielded no statistically significant data, suggesting that the level of both markers is not affected by the two activating compounds. Hence, the decrease in mitochondrial mass upon **36** (THX6) treatment, inferred from TOMM20 level decline, could therefore be primarily attributed to the alteration of mitochondrial biogenesis, rather than to mitochondria degradation events.

Collectively, our data indicate that hClpP activation by **36** (THX6) does not trigger mitochondrial degradation, suggesting that the anticancer potential of this compound might be rather based on mitophagy inhibition. In agreement with our findings is

the observation that some mitophagy proteins, such as BNIP3, exacerbate progression of breast cancer, glioblastoma, and pancreatic tumor. Additionally, proteins not directly involved in mitophagy, such as the proto-oncogene product FAM72A, could also promote tumor progression by stimulating mitophagy in glioma tissues.[41]

2.10. Lipidomic Research. One of the characteristics of tumor cells is altered lipid metabolism, whose specific lipid profile can represent a further interesting aspect with potential diagnostic (i.e., disease stage and grade) and prognostic applications. Furthermore, the synthesis of fatty acids, the desaturation, their absorption, and lipid metabolism in tumor cells may represent a target for cancer therapy.[42] Hence, fatty acid profiles of SU-DIPG-36 and SU-DIPG-50 and, as
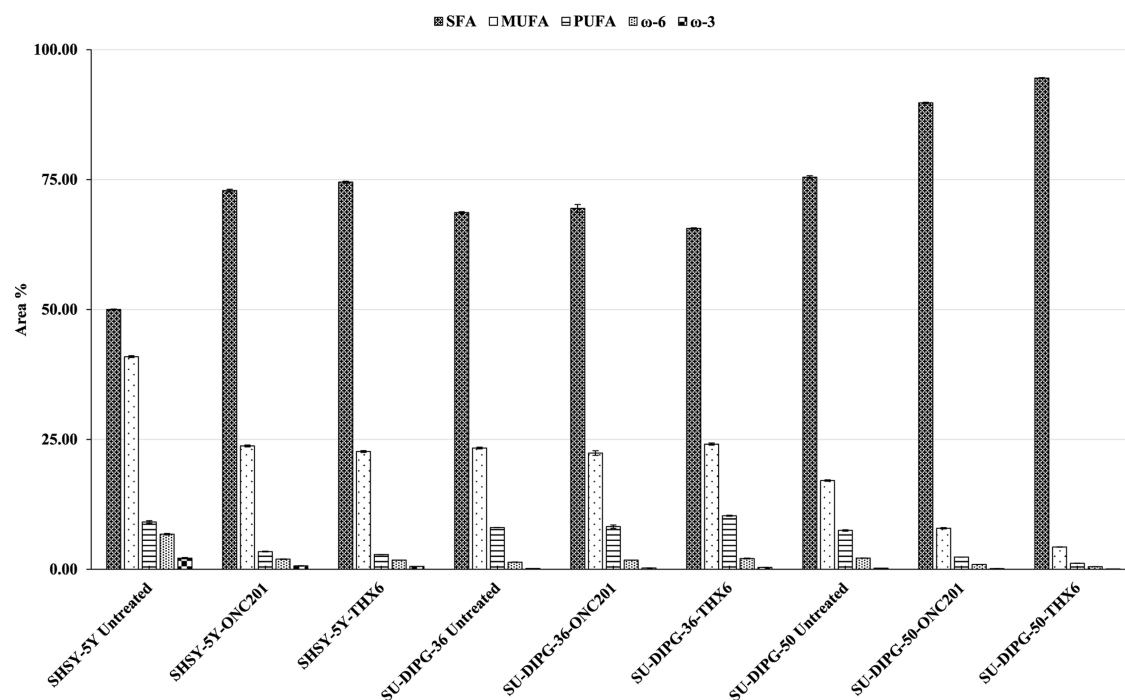
Figure 10. Effect of **ONC201** and **36** (THX6) on SFAs, MUFAs, PUFAs, ω-6, and ω-3 fatty acids in the SU-DIPG-50 cell line.

representative of a non-DIPG tumor, SH-SY5Y, a cloned subline of a neuroblastoma cell line from a metastatic bone tumor, were determined in untreated cells and treated with **ONC201** and **36** (THX6).

To investigate the changes in lipid profiles after cell treatment, GC–MS and GC–FID analyses of the FAMEs were performed. The lipid profiles revealed a total of 34 fatty acids present to different extents in the analyzed samples (untreated cells and treated). Identified FAMEs can be grouped according to chemical structures: saturated fatty acids (SFAs), monounsaturated fatty acids (MUFAs), polyunsaturated fatty acids (PUFAs), and omega-6 (ω-6) and omega-3 (ω-3) fatty acids. FAMEs GC-MS profiles of SH-SY5Y, SU-DIPG-36, and SU-DIPG-50 cell lines untreated and treated with **ONC201** and **36** are depicted in Figures S1–S9. In Table S1 are listed the FAME derivatives detected in untreated and treated cell lines and their relative contents. The untreated SH-SY5Y cell line showed high contents of SFAs due to the presence of abundant amounts of palmitic ($28.69 \pm 0.04\%$) and stearic ($18.01 \pm 0.03\%$) acids. Relevant quantities of MUFAs were also registered with oleic ($28.85 \pm 0.18\%$) and vaccenic ($5.00 \pm 0.03\%$) acids as main components. The family of PUFAs was mainly represented by linoleic ($2.46 \pm 0.05\%$), arachidonic ($2.84 \pm 0.05\%$), and docosahexaenoic ($1.41 \pm 0.08\%$) acids. With regard to the SU-DIPG-36 and SU-DIPG-50 cell lines, similar fatty acid profiles consisting mainly of high amounts of SFA ($68.65 \pm 0.16\%$ and 75.45 ± 0.28 detected in SU-DIPG-36 and SU-DIPG-50, respectively) followed by MUFAs ($23.33 \pm 0.17\%$ in SU-DIPG-36 and $17.07 \pm 0.15\%$ in SU-DIPG-50) were determined; PUFA content ranged from $7.48 \pm 0.14\%$ in SU-DIPG-50 to $8.01 \pm 0.04\%$ in SU-DIPG-36 due to the presence of significant amounts of mead and docosatrienoic acids. Cell treatment with **ONC201** and **36** (THX6) caused the alteration of the composition of the fatty acids, especially those which are prone to structure modification such as PUFAs and MUFAs. On the other hand, SFAs showed a poor susceptibility to oxidations mechanisms after 24 h of **ONC201** and **36** (THX6) treatment

because of the absence of double bonds along the carbon chain. Significant decreases of PUFAs and MUFAs levels were particularly observed in SH-SY5Y and SU-DIPG-50 cell lines treated compared with untreated samples because of reductive mechanisms on cell membranes (Table S1). Surprisingly, this behavior was not found in SU-DIPG-36 after 24 h treatment with both **ONC201** and **36** (THX-6) compounds. This latter finding merits further investigation. Figure 10 shows the changes of SFAs, MUFAs, and PUFAs of the three different cell lines untreated and treated. In addition, the trends of ω-6 and ω-3 fatty acids are included in Figure 10 indicating that the effect of **ONC201** and **36** (THX6) on the cell membranes of the SH-SY5Y and SU-DIPG-50 lines was independent of the position of the double bond along the carbon chain, rather selective toward a higher degree of unsaturation.

3. CONCLUSIONS

TR3 (Figure 1) has been developed as an attempt to simplify the chemical structure of **ONC201** which is currently studied in phase III clinical trials for hGG treatment, even if a very few patients benefit from its administration. In this work, two series (THX and THY) of novel compounds (**33–45**, Schemes 1 and 2) have been developed, using **TR57/TR3** as "lead compounds" and FLAP scores, as activators of the mitochondrial serine protease *h*ClpP, target of **ONC201**. Among all the new synthesized compounds, **36** (THX6) is the most potent identified activator of *h*ClpP showing an EC$_{50}$ of 1.18 μM and a 97% enzyme activation (Table 3). It was also found that it has no affinity for D2R up to 100 μM and an affinity for D3R equal to 51.1 μM, and its interaction with *h*ClpP induces a stabilization of this protease. Moreover, **36** (THX6) has shown a significant cytotoxic effect in the order of submicromolar magnitude (IC$_{50}$ = 0.13 μM) in the highly **ONC201**-resistant cell line SU-DIPG-VI. **36** (THX6) also has an affinity for *h*ClpP higher than **ONC201** as verified with the CETSA experiment and a permeability through membranes comparable to **ONC201**.

In addition, we report preliminary data obtained in a patient-derived DIPG cell line concerning the ability of the novel THPPD-related compound **36** (THX6) to dysregulate the level of some proteins involved in crucial steps of mitochondrial processes such as oxidative phosphorylation, organelle biogenesis, and mitophagy.

The anticancer activity of **36** (THX6) could be linked to mitophagy inhibition. Altering organelle clearance, however, may not always be an effective antitumor strategy due to the dual role (pro-survival and pro-death) of mitophagy in cancer, which depends on a variety of parameters including the unique metabolic environments of different tumors and the stage of tumor progression. Therefore, targeting mitophagy for therapeutic purposes should be done with caution.

It is known that treatment of cancer cells with the imipridone **ONC201** decreases, in addition to subunits of the respiratory chain, also proteins involved in mitochondrial translation, such as translation factors, ribosomal subunits, and assembly factors. Further investigations are currently underway to assess whether the sensitivity of DIPG cells to the imipridone-derivative **36** (THX6) also includes perturbation of mitochondrial translation.

Several questions remain about the molecular mechanisms by which chemically activated *h*ClpP impairs mitochondria. For example, it is not clear how the mitochondrially located protease could affect the level of cytosolic factors or influence the expression of nuclear genes. Although a specific mechanism has not yet been elucidated, it has been proposed that fragments of mitochondrial proteins degraded by hyperactivated *h*ClpP exit mitochondria and promote an integrated stress response as well as the inhibition of cytosolic protein synthesis. The latter event may control the level of nuclear-encoded regulators of mitochondrial biogenesis.

In conclusion, our findings suggest that mitochondrial dysfunction could contribute to **36** (THX6) cellular toxicity. Further investigation is currently underway to validate **36** (THX6) as a novel anticancer drug candidate able to induce cell death by disrupting mitochondrial functions.

4. EXPERIMENTAL SECTION

4.1. Synthetic Methods. Reagents and solvents were purchased from Sigma-Aldrich (Sigma-Aldrich, St. Louis, MO, USA) and used without any further purification. ^{1}H NMR and ^{13}C NMR spectra were recorded on a Bruker 600 MHz or AGILENT 500 MHz spectrometer, and chemical shifts are reported in parts per million (δ), and the following abbreviations were used to explain the multiplicities: s = singlet, d = doublet, t = triplet, q = quartet, m = multiplet, quin = quintuplet, sext = sextet, sep = septet, and b = broad. A Thermo Scientific Nicolet Summit PRO FTIR Spectrometer was employed to obtain the infrared spectra. GC analyses were performed on a HP 6890 model, Series II by using a HP1 column (methyl siloxane; 30 m × 0.32 mm x 0.25 μm film thickness). Analytical thin-layer chromatography was carried out on precoated 0.25 mm thick plates of Kieselgel 60 F254; visualization was accomplished by UV light (254 nm). Column chromatography was accomplished by using silica gel 60 with a particle size distribution 40−63 μm and 230−400 ASTM. GC−MS analyses were performed on an HP 5995C model. High-resolution mass spectrometry (HRMS) analyses were performed using a Bruker microTOF QII mass spectrometer equipped with an electrospray ion source (ESI). High-performance liquid chromatography (HPLC) and electrospray ionization mass spectrometry (ESI−MS) analysis were also carried out. Full characterization data for the newly synthesized compounds are reported below.

All compounds are ≥95% pure by RP-HPLC analysis, except for compound **40** (THX11 with a HPLC purity = 87%). In the ^{1}H NMR spectra of **7−11** is observed in different extent the keto−enolic

equilibrium (Scheme 3). Altogether, 13 new final products were synthesized, analyzed, and tested.

Scheme 3. Keto−Enolic Equilibrium Observed in 7−11 ^{1}H NMR Spectra
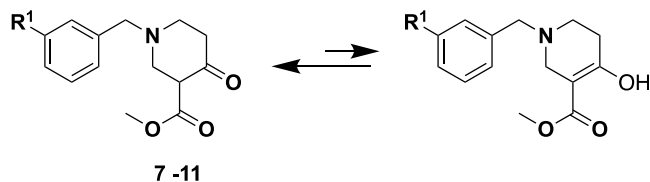
4.2. General Synthesis of 7−11. A mixture of methyl 4-oxopiperidine-3-carboxylate hydrochloride **1** (10.32 mmol) in CH_3OH (100 mL), K_2CO_3 (10.43 mmol), and the appropriate substituted-benzyl bromide **2−6** (10.41 mmol) was stirred at room temperature for 4 h. The reaction mixture was concentrated, extracted with ethyl acetate (3 × 100 mL), and washed with brine. The extracts were dried over anhydrous Na_2SO_4, and the solvent evaporated under reduced pressure to give **7−11**, which were directly used for the next step.

4.3. Methyl 1-(3-cyanobenzyl)-4-oxopiperidine-3-carboxylate (7). Yellow oil; 61% yield. ^{1}H NMR (500 MHz, CDCl$_3$, δ): 11.94 (sharp s, 1H, OH-enolic form), 7.67−7.43 (m, 4H, aromatic protons), 3.77 (s, 2H, NCH$_2$Ar), 3.75 (s, 3H, OCH$_3$), 3.70−3.62 (m, 2H, NCH$_2$CH-keto form and NCH$_2$−enolic form), 3.30−3.14 (m, 1H, CHCO-keto form), 2.70−2.63 (m, 2H, NCH$_2$CH$_2$CO), 2.47−2.43 (m, 2H, NCH$_2$CH$_2$CO). HRMS (ESI) *m/z*: calcd for $[C_{15}H_{16}N_2O_3 + Na]^+$: 295.1055; ESI-MS-MS: 295.1055, 265.0802, 206.1204, 151.0328, 121.0155, 76.9985. ESI-MS *m/z*:: $[C_{15}H_{16}N_2O − H]^-$, 271.1082; ESI-MS-MS: 271.1082, 221.0681, 154.0503, 127.0397, 95.0145, 57.0347.

4.4. Methyl 1-(3-methoxybenzyl)-4-oxopiperidine-3-carboxylate (8). Yellow oil; 63% yield. ^{1}H NMR (500 MHz, CDCl$_3$, δ): 11.94 (sharp s, 1H, OH-enolic form), 7.27−7.21 (m, 1H, aromatic proton), 6.95−6.78 (m, 3H, aromatic protons), 3.83 (s, 3H, ArOCH$_3$), 3.81 (s, 2H, NCH$_2$Ar), 3.80 (s, 3H, OCH$_3$), 3.76 (s, 3H, OCH$_3$), 3.75−3.60 (m, 2H, NCH$_2$CH-keto form and NCH$_2$−enolic form), 3.25−3.20 (m, 1H, CHCO-keto form), 2.68−2.60 (m, 2H, NCH$_2$CH$_2$CO), 2.45−2.38 (m, 2H, NCH$_2$CH$_2$CO). HRMS (ESI) *m/z*: calcd for $[C_{15}H_{19}NO_4 + Na]^+$: 300.1204; ESI-MS-MS: 300.1204,, 268.0933, 151.0372, 121.0643, 91.0537. ESI-MS *m/z*: $[C_{15}H_{19}NO_4 − H]^-$, 276.1254; ESI-MS-MS: 276.1254, 154−0535, 127.0410, 95.0152, 57.0357.

4.5. Methyl 4-oxo-1-(3-(trifluoromethyl)benzyl)piperidine-3-carboxylate (9). Yellow oil; 61% yield. ^{1}H NMR (500 MHz, CDCl$_3$, δ): 11.94 (sharp s, 1H, OH-enolic form)), 7.67−7.43 (m, 4H, aromatic protons), 3.77 (s, 3H, OCH$_3$), 3.75 (s, 2H, NCH$_2$Ar), 3.72−3.60 (m, 2H, NCH$_2$CH-keto form and NCH$_2$−enolic form), 3.27−3.22 (m, 1H, CHCO-keto form), 2.69−2.65 (m, 2H, NCH$_2$CH$_2$CO), 2.47−2.43 (m, 2H, NCH$_2$CH$_2$CO). HRMS (ESI) *m/z*: calcd for $[C_{15}H_{16}F_3NO_3 + Na]^+$: 338.0978; ESI-MS-MS: 338.0978, 288.5759, 238.1071, 151.0360, 119.0097, 96.0771. ESI-MS *m/z*: $[C_{15}H_{16}F_3NO_3 H]^-$, 314.1016; ESI-MS-MS: 314.1016, 226.0486, 154.0519, 127.0406, 85.0304, 57.0352.

4.6. Methyl 1-(3-chlorobenzyl)-4-oxopiperidine-3-carboxylate (10). Yellow oil; 83% yield. ^{1}H NMR (500 MHz, CDCl$_3$, δ): 11.94 (sharp s, 1H, OH-enolic form), 7.66−7.33 (m, 4H, aromatic protons), 3.74 (s, 2H, NCH$_2$Ar), 3.73 (s, 3H, OCH$_3$), 3.72−3.60 (m, 2H, NCH$_2$CH-keto form and NCH$_2$−enolic form), 3.20−3.16 (m, 1H, CHCO-keto form), 2.68−2.60 (m, 2H, NCH$_2$CH$_2$CO), 2.45−2.40 (m, 2H, NCH$_2$CH$_2$CO). HRMS (ESI) *m/z*: calcd for $[C_{14}H_{16}ClNO_3 + Na]^+$: 304.0676; ESI-MS-MS: 304.0676, 272.0454, 176.0257, 151.0360, 125.0158, and 91.0544. ESI-MS *m/z*: $[C_{14}H_{16}ClNO_3 − H]^-$, 280.0748; ESI-MS-MS: 220.0152, 154.0505, 127.0397, 111.0449, 85.0301, 57.0352.

4.7. Methyl 1-(3-nitrobenzyl)-4-oxopiperidine-3-carboxylate (11). Orange oil; 84% yield. ^{1}H NMR (500 MHz, CDCl$_3$, δ):

11.94 (sharp s, 1H, OH-enolic form), 8.24−8.12 (m, 2H, aromatic protons), 7.72−7.63 (m, 1H, aromatic proton), 7.55−7.40 (m, 1H, aromatic proton), 3.75 (s, 2H, NCH$_2$Ar), 3.72 (s, 3H, OCH$_3$), 3.70−3.62 (m, 2H, NCH$_2$CH-keto form and NCH$_2$−enolic form), 3.18−3.16 (s, 1H, CHCO-keto form), 2.66 (t, 2H, J = 10.0 Hz, NCH$_2$CH$_2$CO), 2.43 (t, 2H, J = 10.0 Hz, NCH$_2$CH$_2$CO). HRMS (ESI) m/z calcd for $[C_{14}H_{16}N_2O_5 + Na]^+$: 315.0952; ESI-MS-MS: 315.0952, 285.9841, 151.0339, 151.0360, 112.9584, 76.9976. ESI-MS m/z: $[C_{14}H_{16}N_2O_5 − H]^−$, 291.0987; ESI-MS-MS: 291.0987, 154.0502, 122.0241, 95.0144, 57.0345.

4.8. General Synthesis of 12−16. An ammonia solution (1.68 mL, 25%) and each of **7−11** (7.35 mmol) in ethanol (26 mL) were heated at 70 °C for 5 h. The reaction mixture was concentrated, extracted with methylene chloride (3 × 50 mL), and washed with brine. The extracts were dried over anhydrous Na$_2$SO$_4$, and the solvent evaporated under reduced pressure to give **12−16**. The resulting oil underwent chromatography (silica gel and EtOAc/hexane = 8/2 as the mobile phase) to isolate the products. The product was used in the next step without any further purification.

4.9. Methyl 4-amino-1-(3-cyanobenzyl)-1,2,5,6-tetrahydropyridine-3-carboxylate (12). 50% yield; yellow solid. Mp 73−78 °C. ^{1}H NMR (500 MHz, CDCl$_3$, δ):7.70−7.43 (m, 6H, 4 H, aromatic protons and NH$_2$), 3.74 (s, 2H, NCH$_2$Ar), 3.66 (s, 3H, OCH$_3$), 3.27 (s, 2H, NCH$_2$C), 2.72−2.64 (m, 2H, NCH$_2$CH$_2$), 2.48−2.40 (m, 2H, NCH$_2$CH$_2$). GC−MS (70 eV) (m/z) (rel. int.) 270.10 (58), 256.10 (70), 238.10 (100), 212.20 (57), and 116.20 (84).

4.10. Methyl 4-amino-1-(3-methoxybenzyl)-1,2,5,6-tetrahydropyridine-3-carboxylate (13). Yellow oil; 54% yield. ^{1}H NMR (500 MHz, CDCl$_3$, δ): 7.62−7.40 (m, 6H, 4 H, aromatic protons and NH$_2$), 3.72 (s, 3H, OCH$_3$), 3.68 (s, 2H, NCH$_2$Ar), 3.66 (s, 3H, OCH$_3$), 3.23 (s, 2H, NCH$_2$C), 2.60−2.50 (m, 2H, NCH$_2$CH$_2$), 2.40−2.30 (m, 2H, NCH$_2$CH$_2$). HRMS (ESI) m/z: calcd for $[C_{15}H_{20}N_2O_3 + Na]^+$, 299.1053; ESI-MS-MS: 299.1053, 268.0906, 176.0259, 121.0586, 76.9948, 62.9801.

4.11. Methyl 4-amino-1-(3-(trifluoromethyl)benzyl)-1,2,5,6-tetrahydropyridine-3-carboxylate (14). Yellow oil; 25% yield. ^{1}H NMR (500 MHz, CDCl$_3$, δ): 7.60−7.40 (m, 6H, 4 H, aromatic protons and NH$_2$), 3.68 (s, 2H, NCH$_2$Ar), 3.66 (s, 3H, OCH$_3$), 3.22 (s, 2H, NCH$_2$C), 2.60−2.52 (m, 2H, NCH$_2$CH$_2$), 2.38−2.30 (m, 2H, NCH$_2$CH$_2$). HRMS (ESI) m/z: calcd for $[C_{15}H_{17}F_3N_2O_2 + Na]^+$: 337.1120; ESI-MS-MS: 337.1120, 307.1083, 221.1311, 159.0400, and 76.9967. ESI-MS m/z $[C_{15}H_{17}F_3N_2O_2−H]^−$, 313.1170; ESI-MS-MS: 313.1170, 281.0919.

4.12. Methyl 4-amino-1-(3-chlorobenzyl)-1,2,5,6-tetrahydropyridine-3-carboxylate (15). Yellow oil; 78% yield. ^{1}H NMR: (500 MHz, CDCl$_3$, δ): 7.65−7.40 (m, 6H, 4 H, aromatic protons and NH$_2$), 3.68 (s, 2H, NCH$_2$Ar), 3.66 (s, 3H, OCH$_3$), 3.22 (s, 2H, NCH$_2$C), 2.60−2.50 (m, 2H, NCH$_2$CH$_2$), 2.36−2.30 (m, 2H, NCH$_2$CH$_2$). GC−MS (70 eV) (m/z) (rel. int.) 280.60 (0.9), 270.10 (50), 256.10 (60), 238.10 (92), 212.20 (54), and 116.20 (100).

4.13. Methyl 4-amino-1-(3-nitrobenzyl)-1,2,5,6-tetrahydropyridine-3-carboxylate (16). Yellow oil; 37% yield. ^{1}H NMR (500 MHz, CDCl$_3$, δ): 8.25−7.46 (m, 6H, 4 H, aromatic protons and NH$_2$), 3.71 (s, 2H, NCH$_2$Ar), 3.66 (s, 3H, OCH$_3$), 3.20 (s, 2H, NCH$_2$C), 2.68−2.55 (m, 2H, NCH$_2$CH$_2$), 2.40−2.35 (m, 2H, NCH$_2$CH$_2$). GC−MS (70 eV) (m/z) (rel. int.) 290.80 (13), 290.00 (45), 276.00 (63), 258.10 (100), 232.10 (56), 136.00 (28), 90.10 (49).

4.14. General Synthesis of 33−44. *4.14.1. Step 1: Synthesis of Benzyl Isocyanate (25−32).* The appropriate benzylamine **17−24** (3.10 mmol) was dissolved in EtOAc (12 mL), and at 0 °C, triphosgene (3.06 mmol) was added to the solution. The reaction mixture was stirred at 0 °C for 5 min, and then it was warmed at 80 °C under stirring for 4 h. After this time, the solvent was removed by evaporation under reduced pressure, and the residue immediately used without further purification for the next step because the products are unstable.

4.14.2. Step 2: Conversion of 25−32 into 33−44. To a solution of each **12−16** (3.13 mmol) in toluene (10 mL) were added the appropriate benzyl isocyanate **25−32** and triethylamine (4.35 mmol). The reaction mixture was heated under stirring to 80 °C overnight. The reaction mixture was cooled to room temperature and concentrated in

vacuo. NaOMe (2.78 mmol) was added to the resulting solid dissolved in MeOH (9 mL), and the mixture refluxed overnight. The resulting oil underwent column chromatography on silica gel to give **33−44**.[43,44]

4.14.3. 3-((3-(4-Methylbenzyl)-2,4-dioxo-1,3,4,5,7,8-hexahydropyrido[4,3-d]pyrimidin-6(2H)-yl)methyl)benzonitrile 33 (THX1). Orange solid, mp 170−173 °C; 10% yield; IR (liquid film): 3103, 2919, 2850, 2229, 1594, 1442, 773, 688, 578 cm^{-1}. ^{1}H NMR (500 MHz, CDCl$_3$, δ): 10.26 (s, 1H, NH), 7.69 (s, 1H, aromatic proton), 7.57 (d, 2H. J = 7.75 Hz, aromatic protons), 7.43 (t, 1H, J = 7.7 Hz, aromatic proton), 7.31 (d, 2H, J = 7.9 Hz, aromatic protons), 7.07 (d, 2H, J = 7.9 Hz, aromatic protons), 5.02 (s, 2H, CH$_2$NCO), 3.70 (s, 2H, NCH$_2$Ph), 3.29 (s, 2H, NCH$_2$C), 2.69 (t, 2H, J = 1.1 Hz, NCH$_2$CH$_2$), 2.49 (t, 2H, J = 1.1 Hz, NCH$_2$CH$_2$), 2.28 (s, 3H, Ph−CH$_3$). ^{13}C NMR (125 MHz, CDCl$_3$, δ): 161.90, 152.60, 146.01, 139.50, 137.30, 133.17, 132.24, 131.12, 129.37, 129.25, 128.90, 127,85, 118.62, 106.39, 61.29, 60.38, 48.77, 48.38, 21.11, 21.04. HRMS (ESI) m/z: calcd for $[C_{23}H_{22}N_4O_2+Na]^+$, 409.1630; ESI-MS-MS: 409.1565, 265.0949, 236.0757, 105.0711, 76.9969. ESI-MS m/z: $[C_{23}H_{22}N_4O_2−H]^−$, 385.1663; ESI-MS-MS: 385.1658, 268.1091, 241.0980, 94.0307. The product was isolated by column chromatography (silica gel and EtOAc/hexane = 9/1 as the mobile phase).

4.14.4. 3-((3-(4-Chlorobenzyl)-2,4-dioxo-1,3,4,5,7,8-hexahydropyrido[4,3-d]pyrimidin-6(2H)-yl)methyl)benzonitrile 34 (THX2). Orange solid, mp 173−176 °C; 15% yield. IR (liquid film): 2924, 2853, 2228, 1711, 1641, 1442, 1092, 803, 688 cm^{-1}. ^{1}H NMR (500 MHz, CDCl$_3$, δ): 10.17 (s, 1H, NH), 7.66 (s, 1H, aromatic proton), 7.59−7.50 (m, 6H, aromatic protons), 7.44−7.42 (m, 1H, aromatic proton), 5.11 (s, 2H, CH$_2$NCO), 3.71 (s, 2H, NCH$_2$Ph), 3.29 (s, 2H, NCH$_2$C), 2.70 (t, 2H, J = 5.7 Hz, NCH$_2$CH$_2$), 2.49 (t, 2H, J = 5.5 Hz, NCH$_2$CH$_2$). ^{13}C NMR (125 MHz, CDCl$_3$, δ): 161.99, 152.68, 146.01, 139.53, 133.75, 133.17, 132.24, 131.12, 129.36, 129.24, 128.98, 128.89, 127.81, 118.78, 112.62, 106.39, 61.29, 48.77, 48.38, 43.36, 21.08. HRMS (ESI) m/z: calcd for $[C_{22}H_{19}N_4O_2Cl + Na]^+$, 429.3171. ESI-MS-MS: 311.2920, 125.0139, 76.9968. ESI-MS m/z: $[C_{22}H_{19}N_4O_2Cl−H]^−$, 405.1113. ESI-MS-MS: 405.1107, 288.0541, 261.0434, 218.0373, 94.0300. The product was isolated by column chromatography (silica gel and EtOAc/hexane = 9/1 as the mobile phase).

4.14.5. 3-((3-(4-Nitrobenzyl)-2,4-dioxo-1,3,4,5,7,8-hexahydropyrido[4,3-d]pyrimidin-6(2H)-yl)methyl)benzonitrile 35 (THX4). Light-yellow solid, mp 233−236 °C; 10% yield. IR (liquid film): 3075, 2880, 2226, 1704, 1524, 1344, 687 cm^{-1}. ^{1}H NMR (500 MHz, CDCl$_3$/CD$_3$OD, δ): 8.11−8.09 (m, 2H, aromatic protons), 7.65−7.41 (m, 6H. aromatic protons), 5.10 (s, 2H, CH$_2$NCO), 3.70 (s, 2H, NCH$_2$Ph), 3.25 (s, 2H, NCH$_2$C), 2.74−2.66 (m, 2H, NCH$_2$CH$_2$), 2.56−2.48 (m, 2H, NCH$_2$CH$_2$). ^{13}C NMR (125 MHz, CDCl$_3$/CD3OD, δ): 162.53, 151.41, 147.19, 144.19, 139.23, 133.54, 132.35, 131.18, 129.34, 129.32, 123.50, 118.63, 121.21, 105.33, 61.14, 42.95, 26.27. HRMS (ESI) m/z: calcd for $[C_{22}H_{19}N_5O_4+Na]^+$, 440.1322; ESI-MS-MS: 440.1322, 411.2963, 301.2119, 213.0302, 119.0432, 76.9971. ESI-MS m/z: $[C_{22}H_{19}N_5O_4−H]^−$, 416.1363. ESI-MS-MS: 416.1363, 299.0789, 272.0676, 229.0619, 94.0298. The product was isolated by column chromatography (silica gel and chloroform/methanol = 9.2/0.8 as the mobile phase).

4.14.6. 3-((3-(3,4-Dichlorobenzyl)-2,4-dioxo-1,3,4,5,7,8-hexahydropyrido[4,3-d]pyrimidin-6(2H)-yl)methyl)benzonitrile 36 (THX6). White solid, mp 225−227 °C; 8% yield. IR (liquid film): 2952, 2813, 2230, 1708, 1637, 1445, 1133, 607 cm^{-1}. ^{1}H NMR (500 MHz, CD$_3$OD, δ): 7.62 (s, 1H, aromatic proton), 7.55−7.52 (m, 2H, aromatic protons), 7.46−7.20 (m, 4H, aromatic protons), 4.94 (s, 2H, CH$_2$NCO), 3.71 (s, 2H, NCH$_2$Ph), 3.23 (s, 2H, NCH$_2$C), 2.70−2.62 (m, 2H, NCH$_2$CH$_2$), 2.51−2.43 (m, 2H, NCH$_2$CH$_2$). ^{13}C NMR (125 MHz, CDCl$_3$/CD$_3$OD, δ): 166.28, 155.44, 149.990, 143.20, 140.85, 137.33, 136.27, 136.06, 135.48, 135.11, 134.62, 134.15, 133.25, 122.53, 116.35, 109.43, 65.09, 52.21, 46.45, 30.24. HRMS (ESI) m/z calcd for $[C_{22}H_{18}Cl_2N_4O_2+Na]^+$, 463.0707; ESI-MS-MS m/z: 463.0707, 326.2401, 225.0059, 185.0130, 76.9975). ESI-MS m/z: $[C_{22}H_{18}Cl_2N_4O_2−H]^−$, 439.0728. ESI-MS-MS: 439.0728, 322.0153, 295.0042, 251.9985, 94.0300. The product was isolated by column chromatography (silica gel and EtOAc/hexane = 8/2 as the mobile phase).

4.14.7. 3-((3-(3,5-Bis(trifluoromethyl)benzyl)-2,4-dioxo-1,3,4,5,7,8-hexahydropyrido[4,3-d]pyrimidin-6(2H)-yl)methyl)-benzonitrile 37 (THX7). Light-yellow solid, mp 150−152 °C; 7% yield. IR (liquid film): 2955, 2230, 1713, 1638, 1277, 1170, 1129, 681 cm^{-1}. ^{1}H NMR (500 MHz, CDCl$_3$, δ): 10.12 (s, 1H, NH), 7.92 (s, 2H, aromatic protons), 7.77 (s, 1H, aromatic proton), 7.68 (s, 1H, aromatic proton), 7.58 (d, 2H, J = 7.6 Hz, aromatic protons), 7.44 (t, 2H, J = 7.7 Hz, aromatic protons) 5.14 (s, 2H, CH_2NCO), 3.74 (s, 2H, NCH_2Ph), 3.33 (s, 2H, NCH_2C), 2.79−2.68 (m, 2H, NCH_2CH$_2$), 2.59−2.52 (m, 2H,, NCH$_2$CH_2). ^{13}C NMR (125 MHz, CDCl$_3$, δ): 161.65, 152.43, 145.45, 138.94, 133.14, 133.22, 132.06, 131.77, 131.51, 131.24, 129.65, 129.31, 123.14 (q, J = 271 Hz), 122.06, 121.85 (quin, J = 3.77), 112.69, 106.56, 61.14, 48.61, 48.13, 42.92, 21.09. HRMS (ESI) m/z: calcd for $[C_{24}H_{18}F_6N_4O_2+Na]^+$, 531.1232; ESI-MS-MS m/z: 531.3861, 397.1383, 278.2419, 76.9968. ESI-MS m/z: $[C_{24}H_{18}F_6N_4O_2- H]^-$, 507.1268. ESI-MS-MS: 507.1270, 390.0698, 363.0586, 268.0214, 162.0319. The product was isolated by column chromatography (silica gel and EtOAc/hexane = 9/1 as the mobile phase).

4.14.8. 3-((3-(2-Chloro-5-(trifluoromethyl)benzyl)-2,4-dioxo-1,3,4,5,7,8-hexahydropyrido[4,3-d]pyrimidin-6(2H)-yl)methyl)-benzonitrile 38 (THX8). White solid, mp 204−206 °C; 10% yield. IR (liquid film): 3261, 2811, 2225, 1721, 1614, 1326, 1113, 533 cm^{-1}. ^{1}H NMR (500 MHz, CDCl$_3$/CD$_3$OD, δ): 7.66−7.54 (m, 3H, aromatic protons, 7.46−7.39 (m, 3H, aromatic protons), 7.18 (s, 1H, aromatic proton) 5.16 (s, 2H, CH_2NCO), 3.72 (s, 2H, NCH_2Ph), 3.30 (s, 2H, NCH_2C), 2.83−2.66 (m, 2H, NCH_2CH$_2$), 2.62−2.49 (m, 2H, NCH$_2$CH_2). ^{13}C NMR (125 MHz, CDCl$_3$, δ): 162.35, 151.41, 146.55, 136.80, 135.14, 130.07, 129.40, 129.35, 129.09, 125.12 (q, J = 3.75 Hz), 123.88 (q, J = 270 Hz), 123.59 (q, J = 3.6 Hz), 122.48, 120.31, 118.56, 112.32, 61.00, 48.26, 48.25, 41.25, 26.20. HRMS (ESI) m/z: calcd for C$_{23}$H$_{18}$ClF$_3$N$_4$O$_2$+Na]$^+$, 497.0965. ESI-MS-MS m/z: 497.3215, 353.0279, 239.0203, 185.0126, 76.9979). ESI-MS m/z: $[C_{23}H_{18}ClF_3N_4O_2-H]^-$, 473.0994. ESI-MS-MS: 473.0966, 356.0410, 320.0675, 213.0293, 119.0252. The product was isolated by column chromatography (silica gel and EtOAc/hexane = 9/1 as the mobile phase).

4.14.9. 3-((2,4-Dioxo-3-(4-((trifluoromethyl)thio)benzyl)-1,3,4,5,7,8-hexahydropyrido[4,3-d]pyrimidin-6(2H)-yl)methyl)-benzonitrile 39 (THX10). Light-yellow solid, mp 197−200 °C; 10% yield. IR (liquid film): 2917, 2227, 1707, 1650, 1445, 1132, 688 cm^{-1}. ^{1}H NMR (500 MHz, CDCl$_3$/CD$_3$OD, δ): 7.62 (s, 1H, aromatic proton), 7.55−7.48 (m, 4H, aromatic protons), 7.41−7.36 (m, 3H, aromatic protons), 5.01 (s, 2H, CH_2NCO), 3.68 (s, 2H, NCH_2Ph), 3.25 (s, 2H, NCH_2C), 2.72−2.61 (m, 2H, NCH_2CH$_2$), 2.53−2.44 (m, 2H, NCH$_2$CH_2). ^{13}C NMR (125 MHz, CDCl$_3$, δ): 158.32, 147.59, 141.79, 135.81, 132.31, 129.59, 128.45, 127.37, 126.73, 125.73, 125.39, 124.29, 119.35, 114.67, 108.43, 57.18, 44.58, 44.34, 39.18, 22.28. HRMS (ESI) m/z: calcd for [C$_{23}$H$_{19}$F$_3$N$_4$O$_2$S + Na]$^+$, 495.1093; ESI-MS-MS: 495.1093, 351.0402, 239.0171, 185.0153, 76.9980. ESI-MS m/z: $[C_{23}H_{19}F_3N_4O_2S-H]^-$, 471.1123 ESI-MS-MS: 471.1121, 354.0551, 327.0436, 285.0591, 163.0392, 94.0309. The product was isolated by column chromatography (silica gel and EtOAc/hexane = 7/3 as the mobile phase).

4.14.10. 3-((3-(2,4-Dimethoxybenzyl)-2,4-dioxo-1,3,4,5,7,8-hexahydropyrido[4,3-d]pyrimidin-6(2H)-yl)methyl)benzonitrile 40 (THX11). Yellow semisolid; 15% yield. IR (liquid film): 2927, 2229, 1710, 1640, 1207, 733 cm^{-1}. ^{1}H NMR (500 MHz, CDCl$_3$, δ): 9.66 (s, 1H, NH), 7.66 (s, 1H, aromatic proton), 7.58−7.53 (m, 2H, aromatic protons), 7.45−7.40 (m, 1H, aromatic proton), 6.91 (d, 1H, J = 8.35 Hz, aromatic proton), 6.42 (d, 1H, J = 2.35 Hz, aromatic proton), 6.37 (dd, 1H, J' = 8.35 Hz, J'' = 2.36 Hz, aromatic proton), 5.03 (s, 2H, OCNCH$_2$), 3.80 (s, 3H, OCH_3), 3.74 (s, 3H, OCH_3), 3.70 (s, 2H, PhCH_2N), 3.29 (s, 2H, NCH_2C), 2.69 (t, 2H, J = 5.2 Hz, NCH_2CH$_2$), 2.49 (t, 2H, J = 4.7 Hz, NCH$_2$CH_2). ^{13}C NMR (125 MHz, CDCl$_3$, δ): 161.90, 160.10, 157.98, 152.34, 144.58, 132.91, 131.89, 131.17, 129.38, 127.66, 118.49, 116.37, 112.84, 112.84, 104.38, 98.35, 60.66, 55.73, 48.99, 47.97, 38.41, 30.26, 26.73, 22.90. HRMS (ESI) m/z: calcd for $[C_{24}H_{24}N_4O_4+Na]^+$, 455.1704; ESI-MS-MS: 455.1704, 376.1654, 311.1023, 233.0907, 151.0753, 76.9976. ESI-MS m/z: $[C_{24}H_{24}N_4O_4-H]^-$, 431.1737. ESI-MS-MS: 431.1737, 314.1155, 287.1048, 164.0469, 94.0301. The product was isolated by column

chromatography (silica gel and EtOAc/methanol = 9/1 as the mobile phase).

4.14.11. 6-(3-Methoxybenzyl)-3-(4-(trifluoromethyl)benzyl)-5,6,7,8-tetrahydropyrido[4,3-d]pyrimidine-2,4(1H,3H)-dione 41 (THY1). Yellow semisolid; 6% yield. IR (liquid film): 2939, 1710, 1634, 1322, 1120, 782 cm^{-1}. ^{1}H NMR (500 MHz, CDCl$_3$, δ): 10.06 (s, 1H, NH), 7.54−7.50 (m, 4H, aromatic protons), 7.24 (t, 1H, J = 7.0 Hz, aromatic proton), 6.94−6.88 (m, 2H, aromatic protons), 6.84−6.79 (m, 1H, aromatic proton), 5.10 (s, 2H, OCNCH$_2$), 3.79 (s, 3H, OCH_3), 3.68 (s, 2H, PhCH_2N), 3.35 (s, 2H, NCH_2C), 2.75−2.66 (m, 2H, NCH_2CH$_2$), 2.55−2.44 (m, 2H, NCH$_2$CH_2). ^{13}C NMR (125 MHz, CDCl$_3$, δ): 161.86, 159.78, 152.43, 145.34, 140.60, 129.95, 129.69, 129.44, 129.06 125.31 (q, J = 3.67 Hz), 125.11, 122.95, 121.38, 114.62, 112.94, 62.03, 55.21, 48.72, 47.92, 26.67. HRMS (ESI) m/z: calcd for $[C_{23}H_{22}F_3N_3O_3+Na]^+$, 468.1514; ESI-MS-MS: 468.1514, 439.1048, 326.1303, 159.0372, 121.0610, 81.0281). ESI-MS m/z: $[C_{23}H_{22}F_3N_3O_3-H]^-$, 444.1534. ESI-MS-MS: 444.1534, 322.0804, 295.0695, 252.0656, 94.0294. The product was isolated by column chromatography (silica gel and EtOAc/hexane = 9/1 as the mobile phase).

4.14.12. 6-(3-(Trifluoromethyl)benzyl)-3-(4-(trifluoromethyl)-benzyl)-5,6,7,8-tetrahydropyrido[4,3-d]pyrimidine-2,4(1H,3H)-dione 42 (THY2). Orange solid, mp 137−140 °C; 6% yield. IR (liquid film): 2916, 2849, 1706, 1646, 1325, 1103, 1018, 692 cm^{-1}. ^{1}H NMR (500 MHz, CDCl$_3$ δ): 10.336 (s, 1H, NH), 7.56−7.33 (m, 8H, aromatic protons), 5.05 (s, 2H, OCNCH_2), 3.69 (s, 2H, PhCH_2N), 3.27 (s, 2H, NCH_2C), 2.69−2.61 (m, 2H, NCH_2CH$_2$), 2.51−2.41 (m, 2H, NCH$_2$CH_2). ^{13}C NMR (125 MHz, CDCl$_3$, δ): 161.86, 159.78, 152.43, 146.34, 140.60, 130.20, 129.95, 129.69, 129.44, 129.06, 127.27, 125.35 (q, J = 3.70 Hz), 125.23 (q, J = 3.66 Hz), 122.94, 121.38, 106.64, 62.03, 55.20, 48.72, 47.92, 26.64. HRMS (ESI) m/z calcd for $[C_{23}H_{19}F_6N_3O_2 + Na]^+$, 506.1261; ESI-MS-MS: 506.1261, 467.2950, 324.1752, 213.0070, 185.0124, 76.9972. ESI-MS m/z: $[C_{23}H_{19}F_6N_3O_2-H]^-$, 482.1311. ESI-MS-MS: 482.1311, 322.0816, 295.0705, 252.0657, 94.0302. The product was isolated by column chromatography (silica gel and EtOAc/hexane = 7/3 as the mobile phase).

4.14.13. 6-(3-Chlorobenzyl)-3-(4-(trifluoromethyl)benzyl)-5,6,7,8-tetrahydropyrido[4,3-d]pyrimidine-2,4(1H,3H)-dione 43 (THY3). Light-yellow solid, mp 173−176 °C; 12% yield. IR (liquid film): 2924, 2853, 1712, 1645, 1324, 1123, 1066, 780. cm^{-1}. ^{1}H NMR (500 MHz, CDCl$_3$ δ): 9.67 (s, 1H, NH), 7.52 (s, 4H, aromatic protons), 7.41−7.31 (m, 1H, aromatic proton) 7.24−7.16 (m, 3H, aromatic protons), 5.11 (s, 2H, OCNCH_2), 3.65 (s, 2H, Ph CH_2), 3.31 (s, 2H, NCH_2C), 2.68 (t, 2H, J = 10.0 Hz, NCH_2CH$_2$), 2.48 (t, 2H, J = 10.0 Hz, NCH$_2$CH_2). ^{13}C NMR (125 MHz, CDCl$_3$, δ): 161.89, 152.17, 146.10, 142.59, 139.77, 134.36, 129.69, 129.06, 128.89, 127.64, 127.54, 127.00, 125.40,125.35, 125.30, 135.29, 64.55, 48.73, 48.07, 26.82. HRMS (ESI) m/z calcd for $[C_{22}H_{19}ClF_3N_3O_2+Na]^+$, 472.1008; ESI-MS-MS: 472.1008, 425.0514, 279.0953, 185.0116, 119.0086, 76.9978. ESI-MS m/z: $[C_{22}H_{19}ClF_3N_3O_2-H]^-$, 448.1042. ESI-MS-MS: 448.1042, 322.0809, 295.0699, 252.0639, 94.0300. The product was isolated by column chromatography (silica gel and EtOAc/hexane = 7/3 as the mobile phase).

4.14.14. 6-(3-Nitrobenzyl)-3-(4-(trifluoromethyl)benzyl)-5,6,7,8-tetrahydropyrido[4,3-d]pyrimidine-2,4(1H,3H)-dione 44 (THY4). White solid, mp 198−201 °C; 9% yield. IR (liquid film): 3190, 1714, 1623, 1526, 1323, 1122, 731 cm^{-1}. ^{1}H NMR (500 MHz, CDCl$_3$, δ): 10.13 (s, 1H, NH), 8.24−8.21 (m, 1H, aromatic proton), 8.17−8.11 (m, 1H, aromatic proton), 7.61−7.73 (m, 1H, aromatic proton), 7.54−7.45 (m, 5H, aromatic protons), 5.10 (s, 2H, CH_2NCO), 3.79 (s, 2H, NCH_2Ph), 3.33 (s, 2H, NCH_2C), 2.75−2.72 (m, 2H, NCH_2CH$_2$), 2.55−2.46 (m, 2H, NCH$_2$CH_2). ^{13}C NMR (126 MHz, CDCl$_3$, δ): 162.82, 152.40, 148.48, 146.20, 140.54, 136.85, 134.82, 130.07, 129.64, 129.44, 129.21, 129.06, 125.81, 125.33 (q, J = 6.25 Hz), 124.74, 123.60, 122.63, 61.20, 48.64, 48.32, 43.23, 22.67. HRMS (ESI) m/z: calcd for $[C_{22}H_{19}F_3N_4O_4+Na]^+$, 483.1217; ESI-MS-MS: 483.1217, 425.0514, 239.0198, 185.0127, 120.9865, 76.9965. ESI-MS m/z: $[C_{22}H_{19}F_3N_4O_4-H]^-$, 459.1296. ESI-MS-MS: 459.1296, 322.0813, 295.0699, 252.0651, 121.0403. The product was isolated by column

chromatography (silica gel and EtOAc/hexane = 8/2 as the mobile phase).

4.15. Synthesis of 45 (OMB1). To a solution of **33** (THX1) (0.13 mmol) in 30% NH_3 (3 mL) and CH_3CH_2OH (17 mL) was added Raney-nickel. Raney nickel is activated by treating a block of nickel−aluminum alloy with concentrated sodium hydroxide. The suspension is transferred into an autoclave at room temperature and stirred for 16 h under 5 bar atmospheres of hydrogen. After this time, the reaction mixture was filtrated on Celite, and the solvent was removed by evaporation under reduced pressure. The resulting yellow oil underwent column chromatography (silica gel, CH_2Cl_2/CH_3OH = 9/1 as the mobile phase) to isolate the product.

4.15.1. 6-(3-(Aminomethyl)benzyl)-3-(4-methylbenzyl)-5,6,7,8-tetrahydropyrido[4,3-d]pyrimidine-2,4(1H,3H)-dione **45** *(OMB1).* Light-yellow semisolid; 30% yield. IR (liquid film): 3360, 3190, 2922, 2851, 1632, 1468, 1410, 700 cm^{-1}.^{1}H NMR (500 MHz, CD_3OD, δ): 7.35−7.22 (m, 6H, aromatic protons), 7.07−7.00 (m, 2H, aromatic protons), 4.97 (s, 2H, CH_2NCO), 3.94 (s, 2H, CH_2NH_2), 3.66 (s, 2H, NCH_2Ph), 3.33 (s, 2H, NCH_2C), 2.73−2.65 (m, 2H, NCH_2CH_2), 2.53−2.43 (m, 2H, NCH_2CH_2), 2.24 (s, 3H, CH_3). ^{13}C NMR (126 MHz, CD_3OD, δ): 162.91, 150.56, 146.37, 137.97, 137.06, 135.86, 133.70, 129.38, 129.08, 129.05, 128.83, 128.35, 127.35, 105.19, 77.23, 63.22, 61.86, 43.80, 43.22, 29.50, 23.08, 20.63. HRMS (ESI) m/z: calcd for $[C_{23}H_{26}N_4O_2+Na]^+$, 413.1933; ESI-MS-MS: 413.3182, 340.2208, 239.0197, 185.0122, 131.0042, 76.9970. ESI-MS m/z: $[C_{23}H_{26}N_4O_2$H]$^-$, 389.1982. ESI-MS-MS: 389.2006, 268.1111, 241.1002, 213.1034, 94.0311.

4.16. Computational Studies. Virtual screenings were accomplished using FLAP software (version 2.2.2, build date: 12 February 2020) employing structure-based mode (SBVS)[45,47] This software identifies interaction fields (MIFs), computed in GRID, which depict the interactions between the molecules being analyzed and the specified areas of interest (referred to as pockets) within the crystalline structure.[48] GRID MIFs were generated using four molecular probes: H (shape, steric effects), DRY (hydrophobic interactions), N1 (H-bond donor), and O (H-bond acceptor) interactions. Furthermore, the SBVS mode provides three additional crucial scores for interaction assessment: GLOB-SUM, GLOB-PROD, and Distance. The first two values represent the summation and product of interactions, respectively. The Distance score indicates the overall similarity resulting from a combination of the overlap degrees among the individual probes (H, DRY, O, and N1) of the MIFs calculated for each candidate ligand and binding site. The crystallized structure employed in FLAP is hClpP in complex with **ONC201** (PDB ID: 6DL7; resolution, 2.00 Å) and **TR57** (PDB ID: 7UVN; resolution, 3.11 Å). The GLOB-SUM score served as a reference for evaluating the extent of interaction extent. GLOB-PROD was not utilized due to its limited indicative value, potentially influenced by interaction scores with zero values. Screenings were performed with UCSF Chimera[49,50] (Resource for Biocomputing, Visualization, and Informatics at the University of California, San Francisco, with support from NIH P41-GM103311) with the tools AutoDock Vina Software[51,52] to validate the results obtained by FLAP. PyMOL (The PyMOL Molecular Graphics System, Version 3.0 Schrödinger, LLC.) was also used to identify the coordinates of the pockets docked with the above-mentioned software. This last step was necessary to ensure that the docking took place in a GRID BOX corresponding to the pocket identified by FLAP (Figures S10−S13).[46]

4.17. hClpP Activity Test. FITC-casein assay was performed to assess the potency of the proteolytic activity of hClpP. In a black, flat-bottom, 96-well plate, purified 3 μM hClpP in assay buffer (AB) (50 mM N-(2-hydroxyethyl)piperazine-N′-ethanesulfonic acid (HEPES), pH 7.5, 300 mM KCl, 1 mM DTT, 15% v/v glycerol; AB) preincubated at 37 °C for 15 min was added to 5 μL of the tested compounds in dimethyl sulfoxide (DMSO) at different concentrations (1−100 μM) and incubated for 15 min at 37 °C under shaking. As a control, three wells were filled with 5 μL of DMSO. The kinetic measurement was started after adding 2 μM fluorogenic FITC-casein (Merck, C3777), used as the enzyme substrate. The FITC fluorescence from the hydrolyzed FITC-casein was recorded over 60 min at 37 °C on a Tecan

Infinite M200 Pro (λ_{ex} = 485 nm, λ_{em} = 535 nm, gain: 60). The slope in the linear range between 480 and 1200 s was determined and plotted against time. The EC_{50} for each tested compound was calculated using GraphPad Prism 7.05. Results are reported as the mean of two independent experiments performed in triplicate (Table 3).

4.18. Cellular Thermal Shift Assay. Caco-2 cells were preincubated for 1 h with compounds solubilized in DMSO at a final concentration of 20 μM or DMSO alone as control experiment at the concentration of 0.04%. 100 μL of treated cells was aliquoted into polymerase chain reaction (PCR) tubes (Qiagen) and heated in a SensoQuest 96-well Thermal Cycler (Diatech Pharmacogenetics) at the indicated temperature range for 3 min. Immediately following heating, the aliquots were equilibrated to room temperature (3 min). Subsequently, the cells were rapidly frozen in liquid nitrogen to extract their contents and immediately centrifuged at 14,000 rpm for 20 min at 4 °C to separate soluble from insoluble fragments. The supernatant was carefully aspirated and subjected to Western blotting under reducing conditions. The soluble fractions were solubilized in 2× Laemmli and separated onto 10% Tris-Glycine-SDS minigels (Bio-Rad) and then transferred onto 0.2 μm nitrocellulose membranes using the Trans-Blot Turbo Transfer System (Bio-Rad). Membranes were blocked for 1 h at room temperature with blocking buffer (5% non-fat dry milk, 0.1% Tween-20 in Tris-buffered saline, TBS). The membranes were probed with anti-hClpP polyclonal primary antibody (Product #PA5-52722, Thermo Fisher) at a dilution of 1:1000 at 4 °C overnight, diluted in 5% bovine serum albumin in TBST. After incubation time, membranes were washed ×3 with TBST and incubated with a secondary peroxidase antibody (1:3000 antirabbit) for 1 h at room temperature. After repeated washing, the membranes were treated with the Clarity Western ECL substrate (Bio-Rad) according to the manufacturer's instructions, and the blot was visualized by iBright FL1000 Imaging Systems (Thermo Fisher Scientific).

4.19. Radioligand Binding Studies. *4.19.1. hD2R and hD3R.* Radioligand binding assays were conducted as previously described.[24] Briefly, HEK293 cells stably expressing human D_{2L}R or D3R were grown in a 50:50 mix of Dulbecco's modified Eagle's medium (DMEM) and Ham's F12 culture media, supplemented with 20 mM HEPES, 2 mM L-glutamine, 0.1 mM nonessential amino acids, 1× antibiotic/antimycotic, 10% heat-inactivated fetal bovine serum, and 200 μg/mL hygromycin (Life Technologies, Grand Island, NY) and kept in an incubator at 37 °C and 5% CO_2. Upon reaching 80−90% confluence, cells were harvested using premixed Earle's balanced salt solution with 5 mM EDTA (Life Technologies) and centrifuged at 3,000 rpm for 10 min at 21 °C. The supernatant was removed, and the pellet was resuspended in 10 mL of hypotonic lysis buffer (5 mM $MgCl_2$, 5 mM Tris, pH 7.4 at 4 °C) and centrifuged at 14,500 rpm ($\sim$25,000g) for 30 min at 4 °C. The pellet was then resuspended in binding buffer. Bradford protein assay (Bio-Rad, Hercules, CA) was used to determine the protein concentration. Membranes were diluted to 500 μg/mL, in fresh EBSS binding buffer made by 8.7 g/L Earle's balanced salts without phenol red (US Biological, Salem, MA), 2.2 g/L sodium bicarbonate, pH to 7.4, and stored in a −80 °C freezer for later use. On the test day, each test compound was diluted into half-log serial dilutions using the 30% DMSO vehicle. Membranes were diluted in fresh binding buffer. Radioligand competition experiments were performed in 96-well plates containing 300 μL of fresh binding buffer, 50 μL of the diluted test compound, 100 μL of membranes (20 μg/well total protein for both hD_{2L}R and hD3R), and 50 μL of radioligand diluted in binding buffer ([^{3}H]-N-methylspiperone: 0.4 nM final concentration for all the hD_2-like receptor subtypes; Novandi Chemistry AB). Aliquots of radioligand solution were also quantified accurately in each experiment replicate, to determine how much radioactivity was added, taking into account the experimentally determined counter efficiency. Nonspecific binding was determined using 10 μM (+)-butaclamol (Sigma-Aldrich, St. Louis, MO), and total binding was determined with the 30% DMSO vehicle (3% final concentration). All compound dilutions were tested in triplicate, and the reaction incubated for 60 min at room temperature. The reaction was terminated by filtration through PerkinElmer Uni-Filter-96 GF/C, presoaked for the incubation time in 0.5% polyethylenimine, using a

Brandel 96-Well Plates Harvester Manifold (Brandel Instruments, Gaithersburg, MD). The filters were washed thrice with 3 mL (3 times ∼1 mL/well) of ice-cold binding buffer. A PerkinElmer MicroScint20 Scintillation Cocktail (65 μL) was added to each well, and filters were counted using a PerkinElmer MicroBeta2Microplate Counter. IC_{50} values were determined from dose−response curves, and K_i values were calculated using the Cheng−Prusoff equation.[53] K_d values of the radioligand were determined via separate homologous competitive binding experiments. When a complete inhibition could not be achieved at the highest tested concentrations, K_i values have been extrapolated by constraining the bottom of the dose−response curves (=0% residual specific binding) in the nonlinear regression analysis. These analyses were performed using GraphPad Prism version 9 for Macintosh (GraphPad Software, San Diego, CA). All results were rounded to the third significant figure. K_i values were determined from at least three independent experiments, each performed in triplicate, and are reported as the mean $\pm$ the standard error of the mean (SEM).

4.20. Cell Cultures. Patient-derived DIPG cell cultures (SU-DIPG-36, SU-DIPG-50, SU-DIPG-VI, and HSJD-DIPG-007) were kindly provided by Prof. Michelle Monje of Institutional Review Board (Stanford University and Prof. Javad Nazarian. The cells were cultured as a monolayer in media that was changed once a week at 37 °C in 5% CO_2 by using Tumor Stem Media composed by a 1:1 ratio of DMEM/F12 (Invitrogen)/Neurobasal (-A) (Invitrogen), B27 (-A) (Life Technologies, Milan, Italy), 20 ng/mL human basic fibroblast growth factor (Life Technologies), 20 ng/mL recombinant human epidermal growth factor (Life Technologies), 10 ng/mL platelet-derived growth factor-AA, 10 ng/mL platelet-derived growth factor-BB (Life Technologies), and 20 ng/mL heparin (StemCell Technologies, Milan, Italy).[19] Caco-2 cells were grown in Dulbecco's high-glucose modified Eagle medium, composed of 10% fetal bovine serum, 2 mM glutamine, 100 U/mL penicillin, and 0.1 mg/mL streptomycin (all components purchased from Euroclone, Milan, Italy). Human neuroblastoma SH-SY5Y cells were cultured at 37 °C in 5% CO_2 as in DMEM/F12 (Invitrogen) with an L-glutamine medium composed of 10% FBS, 1% penicillin/streptomycin. SF8628 cells were kindly provided by Prof. Nazarian and were grown in high-glucose DMEM supplemented with 10% FBS, 1× GlutaMAX-I (Invitrogen catalog no. 35030), 1× MEM sodium pyruvate solution (Invitrogen catalog no. 11360), and 1× Pen/Strep (Thermo Fisher cat#15140122).

4.21. Cytotoxic Assay. The *in vitro* cytotoxicity assay was conducted seeding cells at a density of 10,000 cells/well for 24 h in a 96-well plate (Corning, NY, USA) and incubated overnight at 37 °C in a 5% CO_2 atmosphere. Subsequently, the culture medium was replaced with 100 μL of fresh medium containing dilutions of drug ranging from 0.19 to 200 μM and incubated at 37 °C for 72 h. Drug-solvent DMSO was added to each control to evaluate a possible solvent cytotoxicity. After the incubation time with each compound, CCK-8 (10 μL) was added to each well, and after 3−4 h of incubation at 37 °C, the absorbance values at $\lambda = 450$ nm were determined on the Tecan Infinite 200 microplate reader Tecan Infinite 200. IC_{50} values were obtained by using GraphPad Prism software.

4.22. Fatty Acids Profiling by GC−MS and GC−FID Analyses. Total lipids of the cell lines untreated and treated with **ONC201** and **36** (**THX6**) were extracted by using the protocol reported in Stincone et al. with some minor modifications.[54] Briefly, 4 mL of chloroform/methanol (1:2 v/v) was added to the cell culture pellet contained in a 50 mL-conical centrifuge tube; the mixture was homogenized using a vortex mixer for 5 min. Next, 1 mL of chloroform and 2 mL of sodium chloride aqueous solution were added to the extraction mixture; the mixture was homogenized using a vortex mixer and centrifuged (NEYA 16R centrifuge, NEYA ROTORS) at 10,000 rpm for 10 min. The lower chloroform phase containing the lipids was collected by using a Pasteur pipet and transferred into a 2 mL autosampler. Lipids extract in chloroform was dried with an EZ-2 evaporator (EZ-2 Personal-Evaporator, Genevac).

Lipid extracts were derivatized as follows: 500 μL of sodium methoxide methanolic solution (0.5 M, Merck Life Science) was added to the lipid extract, sonicated for 5 min, and heated for 30 min at 95 °C. After cooling, 500 μL of boron trifluoride methanolic solution (14% w/

v, Merck Life Science) was added to the reaction mixture; the solution was heated for 30 min at 95 °C. After cooling, 300 μL of *n*-heptane and 200 μL of water were added to the mixture; the sample was agitated using a vortex mixer for 5 min. After the gravitational separation of the phases, the upper heptane layer containing the FAMEs was collected and injected into the GC systems for the complete characterization.

Separation and identification of FAMEs was performed on a GCMS-QP2020 NX system (Shimadzu, Duisburg, Germany). The injection of the samples was carried out using an AOC-20i autosampler. A split/splitless injector (280 °C) was installed on the GC−MS instrument. The separation of FAMEs was performed on an SLB-IL-60i capillary GC column of 30 m × 0.25 mm ID x 0.20 μm d_f (Merck Life Science). The temperature program was as follows: 70 to 180 °C (10 min) at 3.0 °C min^{-1} and after up to 280 °C at 3.0 °C min^{-1}. Helium was used as a carrier gas at a constant linear velocity of 30 cm s^{-1} (inlet pressure 31.7 kPa). Volume injection of 1.0 μL (split ratio 1:10). MS parameters were as follows: mass range 40−550 amu; event time 100 ms; ion source temperature: 220 °C, interface temperature: 250 °C. GC−MS solution software (version 4.50, Shimadzu) was used for data collection and handling. The identification of FAMEs was performed by using two different identification criteria: mass spectral similarity (over 85%) and linear retention index (LRI) with a tolerance window of ±10 units of LRI. In such a respect, a homologue series of C4−C24 even carbon saturated FAMEs (Merck Life Science) were used for calculating LRIs. The identification of FAMEs was carried out by using a commercial database, namely, LIPIDS GC−MS Library (version 1.0, Shimadzu).

FAMEs quantification was carried out on a Nexis GC-2030 high-performance capillary gas chromatograph (Shimadzu) coupled to a flame ionization detector (FID). The instrument was equipped with a split/splitless injector (280 °C) and an AOC-20i autosampler. The capillary column, temperature program, and gas linear velocity were the same as described for GC−MS instrumentation, except for the inlet pressure of the carrier gas (103.5 kPa). FID temperature was set at 280 °C (sampling rate 40 ms); gas flows were 40 mL min^{-1} for hydrogen, 10 mL min^{-1} for make up (nitrogen), and 400 mL min^{-1} for air. Data were acquired and processed through LabSolutions software (ver. 5.92, Shimadzu). Each sample was injected in triplicate for major data precision.

4.23. Drug Transport Experiments. The experiment started with the preparation of the Caco-2 monolayer, which occurred by seeding the cells (20,000/well) in Millicell plates (Millipore, Milan, Italy). Its growth was followed for 21 days by changing the medium occasionally and measuring its transepithelial electrical resistance daily using an epithelial voltohmmeter (Millicell-ERS)[28] until at least 1000W was reached. After 21 days, the plate was washed twice with Hank's balanced salt solution (HBSS) (Invitrogen). After the second wash, the wells were filled with buffer and the plate was kept at 37 °C for 30 min. After the incubation time, the HBSS buffer was replaced with the solutions of the compounds to be tested at a concentration equal to 10^{-4} M. The plates were placed in an incubator at 37 °C for 2 h. The apparent permeability (P_{app}) was calculated in units of nm/s.

4.24. Immunoblotting Analyses. Western blots were performed as previously described.[55] Briefly, whole cell proteins (40 μg) from either untreated or compound **36** (**THX6**)-treated cells were solubilized in 1× Laemmli buffer and separated onto 12% Tris-Glycine-SDS minigels. Immunodetection was carried out by the following primary antibodies: anti-*h*ClpX, anti-*h*ClpP, anti-NRF1, anti-COI, anti-ATP5A, anti-Parkin, anti-BNIP3, and anti-NIX (all from Abcam); anti-TOMM20 (Proteintech); anti-SDHA (Millipore); anti-TFAM (Cell Signaling Technology); anti-β-actin (Sigma-Aldrich). Chemiluminescent detection was performed using the Clarity Western ECL substrate (Bio-Rad), and signals were revealed by the ChemiDoc MP Imaging System (Bio-Rad).

4.25. Relative Quantitation of the mtDNA Level. For DNA isolation, SU-DIPG-36 untreated and treated cells were harvested from 10 cm tissue culture dishes and pelleted by centrifugation. Pellets were resuspended in TE solution (10 mM Tris, pH 7.4; 1 mM EDTA), followed by addition of 1% SDS and 2 mg/mL proteinase K. After overnight incubation at 37 °C with gentle shaking, DNA was phenol-extracted, precipitated, and resuspended in sterile water. Mitochondrial

Q

DNA levels were measured by real-time quantitative PCR using the SsoAdvanced Universal SYBR Green Supermix (Bio-Rad) and the Applied Biosystems 7500 Fast Real-Time PCR System (Thermo Fisher Scientific). Primer sequences used to amplify specific regions within either the mitochondrial genome (target) or 18S rRNA gene (reference) were as follows: ND4-for 5′-CCATTCTCCTCC-TATCCCTCAAC-3′; ND4-rev 5′-CACAATCTGATGTTTTGGT-TAAACTATATTT-3′; 18S-for 5′-GTAACCCGTTGAACCCCATT-3′; 18S-rev 5′-CCATCCAATCGGTAGTAGCG-3′. Melting curve analysis was performed to ensure the amplification specificity; the relative quantification was carried out according to the formula $R = (E_T)^{\Delta Ct,T}/(E_C)^{\Delta Ct,C}$ where E_T and E_C indicate the amplification efficiencies on the mt-ND4 (target) and 18S rRNA gene (control), respectively.[56]

■ ASSOCIATED CONTENT

ⓢ Supporting Information

The Supporting Information is available free of charge at https://pubs.acs.org/doi/10.1021/acs.jmedchem.4c01723.

> Kinetic traces and activity plots used to calculate EC_{50} values for the target compounds and references; cytotoxic curves of the target compounds and references; ^{1}H NMR, ^{13}C NMR, and FTIR spectra; HPLC of the target compounds and references; GC−MS chromatograms; and summary of FAMEs data (PDF)
>
> Molecular formula strings (CSV)
>
> AutoDock VINA predicted poses of 6dl7 (MP4)
>
> AutoDock VINA predicted poses of 7uvn (MP4)

■ AUTHOR INFORMATION

Corresponding Authors

Maria Grazia Perrone − *Research Laboratory for Woman and Child Health, Department of Pharmacy—Pharmaceutical Sciences, University of Bari Aldo Moro, 70125 Bari, Italy;* ⓞ orcid.org/0000-0003-4195-5228; Email: mariagrazia.perrone@uniba.it

Antonio Scilimati − *Research Laboratory for Woman and Child Health, Department of Pharmacy—Pharmaceutical Sciences, University of Bari Aldo Moro, 70125 Bari, Italy;* ⓞ orcid.org/0000-0003-2740-6425; Email: antonio.scilimati@uniba.it

Authors

Morena Miciaccia − *Research Laboratory for Woman and Child Health, Department of Pharmacy—Pharmaceutical Sciences, University of Bari Aldo Moro, 70125 Bari, Italy;* ⓞ orcid.org/0000-0002-0727-6435

Olga Maria Baldelli − *Research Laboratory for Woman and Child Health, Department of Pharmacy—Pharmaceutical Sciences, University of Bari Aldo Moro, 70125 Bari, Italy*

Cosimo G. Fortuna − *Laboratory of Molecular Modelling and Heterocyclic Compounds ModHet, Department of Chemical Sciences, University of Catania, 95125 Catania, Italy*

Gianfranco Cavallaro − *Laboratory of Molecular Modelling and Heterocyclic Compounds ModHet, Department of Chemical Sciences, University of Catania, 95125 Catania, Italy;* ⓞ orcid.org/0009-0009-6759-3860

Domenico Armenise − *Research Laboratory for Woman and Child Health, Department of Pharmacy—Pharmaceutical Sciences, University of Bari Aldo Moro, 70125 Bari, Italy*

Anselma Liturri − *Research Laboratory for Woman and Child Health, Department of Pharmacy—Pharmaceutical Sciences, University of Bari Aldo Moro, 70125 Bari, Italy*

Savina Ferorelli − *Research Laboratory for Woman and Child Health, Department of Pharmacy—Pharmaceutical Sciences, University of Bari Aldo Moro, 70125 Bari, Italy*

Denise Muñoz − *Helen Diller Family Comprehensive Cancer Center, University of California San Francisco, San Francisco, California 94115, United States*

Alessandro Bonifazi − *Medicinal Chemistry Section, Molecular Targets and Medications Discovery Branch, National Institute on Drug Abuse, Intramural Research Program, National Institutes of Health, Baltimore, Maryland 21224, United States;* ⓞ orcid.org/0000-0002-7306-0114

Francesca Rizzo − *Department of Biosciences, Biotechnologies and Environment, University of Bari Aldo Moro, 70125 Bari, Italy;* ⓞ orcid.org/0000-0002-1736-8966

Antonella Cormio − *Department of Precision and Regenerative Medicine and Ionian Area, University of Bari Aldo Moro, 70124 Bari, Italy*

Silvana Filieri − *Department of Translational Biomedicine and Neuroscience, University of Bari Aldo Moro, 70124 Bari, Italy*

Giuseppe Micalizzi − *Messina Institute of Technology c/o Department of Chemical, Biological, Pharmaceutical and Environmental Sciences, former Veterinary School, University of Messina, Messina 98168, Italy*

Paola Dugo − *Messina Institute of Technology c/o Department of Chemical, Biological, Pharmaceutical and Environmental Sciences, former Veterinary School, University of Messina, Messina 98168, Italy; Chromaleont s.r.l., c/o Department of Chemical, Biological, Pharmaceutical and Environmental Sciences, former Veterinary School, University of Messina, Messina 98168, Italy*

Luigi Mondello − *Messina Institute of Technology c/o Department of Chemical, Biological, Pharmaceutical and Environmental Sciences, former Veterinary School, University of Messina, Messina 98168, Italy; Chromaleont s.r.l., c/o Department of Chemical, Biological, Pharmaceutical and Environmental Sciences, former Veterinary School, University of Messina, Messina 98168, Italy*

Anna Maria Sardanelli − *Department of Translational Biomedicine and Neuroscience, University of Bari Aldo Moro, 70124 Bari, Italy*

Francesco Bruni − *Department of Biosciences, Biotechnologies and Environment, University of Bari Aldo Moro, 70125 Bari, Italy*

Paola Loguercio Polosa − *Department of Biosciences, Biotechnologies and Environment, University of Bari Aldo Moro, 70125 Bari, Italy*

Complete contact information is available at:
https://pubs.acs.org/10.1021/acs.jmedchem.4c01723

Author Contributions

[∥]M.M., O.M.B., and C.G.F. contributed equally to the experimental part of the work. The manuscript was written through contribution of all authors. M.G.P. is co-last author with A.S. All authors have given approval to the final version of the manuscript.

Notes

The authors declare no competing financial interest.

■ ACKNOWLEDGMENTS

■ ABBREVIATIONS

BBB, blood—brain barrier; Caco-2, colon carcinoma cell line; CETSA, cellular thermal shift assay; DIPG, diffuse intrinsic pontine glioma; EDG, electron-donating group; ESI, electro-spray ion source; EWG, electron-withdrawing group; FAME, fatty acid methyl ester; FITC, fluorescein-isothiocyanate; FLAP, fingerprints for ligands and proteins; HBSS, Hank's balanced salt solution; hClpP, human caseinolytic protease P; hGG, high-grade glioma; HRMS, high-resolution mass spectrometry; MIFs, molecular interaction fields; mt, mitochondrial; MUFAs, monounsaturated fatty acids; P_{app}, apparent permeability; PDB, protein data bank; PUFAs, polyunsaturated fatty acids; SBVS, structure-based virtual screening; SFAs, saturated fatty acids; THPPDs, tetrahydropyridopyrimidindiones; TLC, thin-layer chromatography

■ REFERENCES

(1) Perrone, M. G.; Ruggiero, A.; Centonze, A.; Carrieri, A.; Ferorelli, S.; Scilimati, A. Diffuse Intrinsic Pontine Glioma (DIPG): Break-through and Clinical Perspective. *Curr. Med. Chem.* **2021**, *28*, 3287–3317.

(2) Mandorino, M.; Maitra, A.; Armenise, D.; Baldelli, O. M.; Miciaccia, M.; Ferorelli, S.; Perrone, M. G.; Scilimati, A. Pediatric Diffuse Midline Glioma H3K27-Altered: From Developmental Origins to Therapeutic Challenges. *Cancers* **2024**, *16*, 1814.

(3) Madhukar, N. S.; Khade, P. K.; Huang, L.; Gayvert, K.; Galletti, G.; Stogniew, M.; Allen, J. E.; Giannakakou, P.; Elemento, O. A Bayesian machine learning approach for drug target identification using diverse data types. *Nat. Commun.* **2019**, *10*, 5221.

(4) Allen, J. E.; Krigsfeld, G.; Mayes, P. A.; Patel, L.; Dicker, D. T.; Patel, A. S.; Dolloff, N. G.; Messaris, E.; Scata, K. A.; Wang, W.; et al. Dual inactivation of Akt and ERK by TIC10 signals Foxo3a nuclear translocation, TRAIL gene induction, and potent antitumor effects. *Sci. Transl. Med.* **2013**, *5* (171), 171ra117.

(5) Graves, P. R.; Aponte-Collazo, L. J.; Fennell, E. M. J.; Graves, A. C.; Hale, A. E.; Dicheva, N.; Herring, L. E.; Gilbert, T. S. K.; East, M. P.; McDonald, I. M.; et al. Correction to "Mitochondrial Protease ClpP Is a Target for the Anticancer Compounds ONC201 and Related Analogues. *ACS Chem. Biol.* **2022**, *17*, 2377–2378.

(6) https://clinicaltrials.gov/study/NCT05580562; accessed 2/19/2025.

(7) Wong, K. S.; Houry, W. A. Chemical Modulation of Human Mitochondrial ClpP: Potential Application in Cancer Therapeutics. *ACS Chem. Biol.* **2019**, *14*, 2349–2360.

(8) Mabanglo, M. F.; Wong, K. S.; Barghash, M. M.; Leung, E.; Chuang, S. H. W.; Ardalan, A.; Majaesic, E. M.; Wong, C. J.; Zhang, S.; Lang, H.; et al. Potent ClpP agonists with anticancer properties bind with improved structural complementarity and alter the mitochondrial N-terminome. *Structure* **2023**, *31*, 185–200e110.

(9) Nouri, K.; Feng, Y.; Schimmer, A. D. Mitochondrial ClpP serine protease-biological function and emerging target for cancer therapy. *Cell Death Dis.* **2020**, *11*, 841.

(10) LaBreck, C. J.; May, S.; Viola, M. G.; Conti, J.; Camberg, J. L. The Protein Chaperone ClpX Targets Native and Non-native Aggregated Substrates for Remodeling, Disassembly, and Degradation with ClpP. *Front. Mol. Biosci.* **2017**, *4*, 26.

(11) Wu, G.; Xiong, Q.; Wei, X.; Wang, Y.; Hu, X.; He, G.; Liu, L.; Lai, Q.; Dai, Z.; Anushesh, D.; et al. Mitochondrial unfolded protein response gene CLPP changes mitochondrial dynamics and affects mitochondrial function. *PeerJ* **2019**, *7*, No. e7209.

(12) Free, R. B.; Cuoco, C. A.; Xie, B.; Namkung, Y.; Prabhu, V. V.; Willette, B. K. A.; Day, M. M.; Sanchez-Soto, M.; Lane, J. R.; Laporte, S. A.; et al. Pharmacological Characterization of the Imipridone Anticancer Drug ONC201 Reveals a Negative Allosteric Mechanism of Action at the D. *Mol. Pharmacol.* **2021**, *100*, 372–387.

(13) Huang, J.; Zhang, J.; Luo, B.; Qiao, W.; Qiu, Z.; Song, R.; Dai, Z.; Sui, J.; Xu, X.; Ruan, S.; et al. Discovery of a Novel Series of Imipridone Compounds as. *J. Med. Chem.* **2022**, *65*, 7629–7655.

(14) Zhang, J.; Luo, B.; Sui, J.; Qiu, Z.; Huang, J.; Yang, T.; Luo, Y. IMP075 targeting ClpP for colon cancer therapy in vivo and in vitro. *Biochem. Pharmacol.* **2022**, *204*, 115232.

(15) Fennell, E. M. J.; Aponte-Collazo, L. J.; Wynn, J. D.; Drizyte-Miller, K.; Leung, E.; Greer, Y. E.; Graves, P. R.; Iwanowicz, A. A.; Ashamalla, H.; Holmuhamedov, E.; et al. Characterization of TR-107, a novel chemical activator of the human mitochondrial protease ClpP. *Pharmacol. Res. Perspect.* **2022**, *10*, No. e00993.

(16) Halgas, O.; Zarabi, S. F.; Schimmer, A.; Pai, E. F. Human mitochondrial ClpP in complex with ONC201 (TIC10), 2019 https://www.rcsb.org/structure/6DL7; accessed 02/19/2025.

(17) Mabanglo, M. F., Houry, W. A. Crystal structure of human ClpP protease in complex with TR-57, 2023 https://www.rcsb.org/structure/7UVN.

(18) Leung, E.; Datti, A.; Cossette, M.; Goodreid, J.; McCaw, S. E.; Mah, M.; Nakhamchik, A.; Ogata, K.; El Bakkouri, M.; Cheng, Y. Q.; et al. Activators of cylindrical proteases as antimicrobials: identification and development of small molecule activators of ClpP protease. *Chem. Biol.* **2011**, *18*, 1167–1178.

(19) Miciaccia, M.; Rizzo, F.; Centonze, A.; Cavallaro, G.; Contino, M.; Armenise, D.; Baldelli, O. M.; Solidoro, R.; Ferorelli, S.; Scarcia, P.; et al. Harmaline to Human Mitochondrial Caseinolytic Serine Protease Activation for Pediatric Diffuse Intrinsic Pontine Glioma Treatment. *Pharmaceuticals* **2024**, *17*, 135.

(20) Daina, A.; Michielin, O.; Zoete, V. SwissADME: a free web tool to evaluate pharmacokinetics, drug-likeness and medicinal chemistry friendliness of small molecules. *Sci. Rep.* **2017**, *7*, 42717.

(21) Zhi-wei, G.; Ngooi, T. K.; Scilimati, A.; Fulling, G.; Sih, C. J. Macrocyclic lactones via biocatalysis in non-aqueous media. *Tetrahedron Lett.* **1988**, *29*, 5583–5586.

(22) Di Nunno, L.; Franchini, C.; Scilimati, A.; Sinicropi, M. S.; Tortorella, P. Chemical and chemoenzymatic routes to 1-(benzothiazol-2-ylsulfanyl)-3-chloropropan-2-ol, a precursor of drugs with potential β-blocker activity. *Tetrahedron:Asymmetry* **2000**, *11*, 1571−1583.

(23) Prabhu, V. V.; Morrow, S.; Rahman Kawakibi, A.; Zhou, L.; Ralff, M.; Ray, J.; Jhaveri, A.; Ferrarini, I.; Lee, Y.; Parker, C.; et al. ONC201 and imipridones: Anti-cancer compounds with clinical efficacy. *Neoplasia* **2020**, *22*, 725−744.

(24) Bonifazi, A.; Saab, E.; Sanchez, J.; Nazarova, A. L.; Zaidi, S. A.; Jahan, K.; Katritch, V.; Canals, M.; Lane, J. R.; Newman, A. H. Pharmacological and Physicochemical Properties Optimization for Dual-Target Dopamine D. *J. Med. Chem.* **2023**, *66*, 10304−10341.

(25) Jackson, E. R.; Duchatel, R. J.; Staudt, D. E.; Persson, M. L.; Mannan, A.; Yadavilli, S.; Parackal, S.; Game, S.; Chong, W. C.; Jayasekara, W. S. N.; et al. ONC201 in Combination with Paxalisib for the Treatment of H3K27-Altered Diffuse Midline Glioma. *Cancer Res.* **2023**, *83*, 2421−2437.

(26) Maitra, A.; Mandorino, M.; Armenise, D.; Baldelli, O. M.; Miciaccia, M.; Ferorelli, S.; Papusha, L.; Druy, A.; Perrone, M. G.; Scilimati, A. Decoding Gene Expression Changes in Pediatric Cerebral Tumors: Before and After Radiotherapy. *Med. Res. Rev.* **2024**. Submitted for publication. .

(27) Lee, A.; Maranto, C.; Foster, S.; Morrow, S.; Allen, J. E.; Lanier, R.; Sethna, P.; Prabhu, V. Abstract 4914: Role of ClpP in the anti-cancer effects of imipridone ONC201 and ONC206. *Cancer Res.* **2023**, *83* (7_Supplement), 4914.

(28) Liantonio, A.; Gramegna, G.; Camerino, G. M.; Dinardo, M. M.; Scaramuzzi, A.; Potenza, M. A.; Montagnani, M.; Procino, G.; Lasorsa, D. R.; Mastrofrancesco, L.; et al. In-vivo administration of CLC-K kidney chloride channels inhibitors increases water diuresis in rats: a new drug target for hypertension? *J. Hypertens.* **2012**, *30*, 153−167.

(29) Teodori, E.; Contino, M.; Riganti, C.; Bartolucci, G.; Braconi, L.; Manetti, D.; Romanelli, M. N.; Trezza, A.; Athanasios, A.; Spiga, O.; et al. Design, synthesis and biological evaluation of stereo- and regioisomers of amino aryl esters as multidrug resistance (MDR) reversers. *Eur. J. Med. Chem.* **2019**, *182*, 111655.

(30) Perrone, M. G.; Santandrea, E.; Bleve, L.; Vitale, P.; Colabufo, N. A.; Jockers, R.; Milazzo, F. M.; Sciarroni, A. F.; Scilimati, A. Stereospecific synthesis and bio-activity of novel beta(3)-adrenoceptor agonists and inverse agonists. *Bioorg. Med. Chem.* **2008**, *16*, 2473−2488.

(31) Perrone, M. G.; Santandrea, E.; Dell'Uomo, N.; Giannessi, F.; Milazzo, F. M.; Sciarroni, A. F.; Scilimati, A.; Tortorella, V. Synthesis and biological evaluation of new clofibrate analogues as potential PPARalpha agonists. *Eur. J. Med. Chem.* **2005**, *40*, 143−154.

(32) Jacques, S.; van der Sloot, A. M.; C Huard, C.; Coulombe-Huntington, J.; Tsao, S.; Tollis, S.; Bertomeu, T.; Culp, E. J.; Pallant, D.; Cook, M. A.; et al. Imipridone Anticancer Compounds Ectopically Activate the ClpP Protease and Represent a New Scaffold for Antibiotic Development. *Genetics* **2020**, *214*, 1103−1120.

(33) Ferrarini, I.; Louie, A.; Zhou, L.; El-Deiry, W. S. ONC212 is a Novel Mitocan Acting Synergistically with Glycolysis Inhibition in Pancreatic Cancer. *Mol. Cancer Ther.* **2021**, *20*, 1572−1583.

(34) Ishizawa, J.; Zarabi, S. F.; Davis, R. E.; Halgas, O.; Nii, T.; Jitkova, Y.; Zhao, R.; St-Germain, J.; Heese, L. E.; Egan, G.; et al. Mitochondrial ClpP-Mediated Proteolysis Induces Selective Cancer Cell Lethality. *Cancer Cell* **2019**, *35*, 721−737e729.

(35) Greer, Y. E.; Porat-Shliom, N.; Nagashima, K.; Stuelten, C.; Crooks, D.; Koparde, V. N.; Gilbert, S. F.; Islam, C.; Ubaldini, A.; Ji, Y.; et al. ONC201 kills breast cancer cells. *Oncotarget* **2018**, *9*, 18454−18479.

(36) Abu Shelbayeh, O.; Arroum, T.; Morris, S.; Busch, K. B. PGC-1α Is a Master Regulator of Mitochondrial Lifecycle and ROS Stress Response. *Antioxidants* **2023**, *12*, 1075.

(37) Mabanglo, M. F.; Bhandari, V.; Houry, W. A. Substrates and interactors of the ClpP protease in the mitochondria. *Curr. Opin. Chem. Biol.* **2022**, *66*, 102078.

(38) Fischer, F.; Langer, J. D.; Osiewacz, H. D. Identification of potential mitochondrial CLPXP protease interactors and substrates suggests its central role in energy metabolism. *Sci. Rep.* **2015**, *5*, 18375.

(39) Knuppertz, L.; Osiewacz, H. D. Autophagy compensates impaired energy metabolism in CLPXP-deficient Podospora anserina strains and extends healthspan. *Aging Cell* **2017**, *16*, 704−715.

(40) Wang, S.; Dougan, D. A. The Direct Molecular Target for Imipridone ONC201 Is Finally Established. *Cancer Cell* **2019**, *35*, 707−708.

(41) Zheng, Y.; Zhang, D.; Su, L.; Wen, Y.; Wang, Y. FAM172A supervises ER (endoplasmic reticulum) stress-triggered autophagy in the epidural fibrosis process. *JOR Spine* **2022**, *5* (2), No. e1203.

(42) Terry, A. R.; Hay, N. Emerging targets in lipid metabolism for cancer therapy. *Trends Pharmacol. Sci.* **2024**, *45*, 537−552.

(43) Iwanowicz, E. J. Protein kinase regulators. WO 2018031990 A1; Madera Therapeutics, LLC.

(44) Iwanowicz, E. J. Use of Caseinolytic protease P function as a biomarker of drug response ti imipridone-like agents. WO 2020176654 A1; Madera Therapeutics, LLC.

(45) Carosati, E.; Sciabola, S.; Cruciani, G. Hydrogen bonding interactions of covalently bonded fluorine atoms: from crystallographic data to a new angular function in the GRID force field. *J. Med. Chem.* **2004**, *47*, 5114−5125.

(46) Perrone, M. G.; Vitale, P.; Miciaccia, M.; Ferorelli, S.; Centonze, A.; Solidoro, R.; Munzone, C.; Bonaccorso, C.; Fortuna, C. G.; Kleinmanns, K.; et al. Fluorochrome Selection for Imaging Intraoperative Ovarian Cancer Probes. *Pharmaceuticals* **2022**, *15*, 668.

(47) Perrone, M. G.; Miciaccia, M.; Vitale, P.; Ferorelli, S.; Araújo, C. D. C. B.; de Almeida, G. S.; Souza Domingos, T. F.; da Silva, L. C. R. P.; de Pádula, M.; Cabral, L. M.; et al. An attempt to chemically state the cross-talk between monomers of COX homodimers by double/hybrid inhibitors mofezolac-spacer-mofezolac and mofezolac-spacer-arachidonic acid. *Eur. J. Med. Chem.* **2021**, *209*, 112919.

(48) Goodford, P. J. A computational procedure for determining energetically favorable binding sites on biologically important macromolecules. *J. Med. Chem.* **1985**, *28*, 849−857.

(49) Pettersen, E. F.; Goddard, T. D.; Huang, C. C.; Couch, G. S.; Greenblatt, D. M.; Meng, E. C.; Ferrin, T. E. UCSF Chimera−a visualization system for exploratory research and analysis. *J. Comput. Chem.* **2004**, *25*, 1605.

(50) Butt, S. S.; Badshah, Y.; Shabbir, M.; Rafiq, M. Molecular Docking Using Chimera and Autodock Vina Software for Non-bioinformaticians. *JMIR Bioinform Biotechnol.* **2020**, *1*, No. e14232.

(51) Eberhardt, J.; Santos-Martins, D.; Tillack, A. F.; Forli, S. AutoDock Vina 1.2.0: New Docking Methods, Expanded Force Field, and Python Bindings. *J. Chem. Inf. Model.* **2021**, *61*, 3891−3898.

(52) Trott, O.; Olson, A. J. AutoDock Vina: improving the speed and accuracy of docking with a new scoring function, efficient optimization and multithreading. *J. Comput. Chem.* **2010**, *31*, 455−461.

(53) Cheng, Y.; Prusoff, W. H. Relationship between the inhibition constant ($K1$) and the concentration of inhibitor which causes 50% inhibition ($I50$) of an enzymatic reaction. *Biochem. Pharmacol.* **1973**, *22* (23), 3099−3108.

(54) Stincone, P.; Fonseca Veras, F.; Micalizzi, G.; Donnarumma, D.; Vitale Celano, G.; Petras, D.; de Angelis, M.; Mondello, L.; Brandelli, A. Listeria monocytogenes exposed to antimicrobial peptides displays differential regulation of lipids and proteins associated to stress response. *Cell. Mol. Life Sci.* **2022**, *79*, 263.

(55) Loguercio Polosa, P.; Capriglia, F.; Bruni, F. Molecular Investigation of Mitochondrial RNA19 Role in the Pathogenesis of MELAS Disease. *Life* **2023**, *13*, 1863.

(56) Pfaffl, M. W. A new mathematical model for relative quantification in real-time RT-PCR. *Nucleic Acids Res.* **2001**, *29*, No. e45.